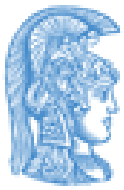

HELLENIC REPUBLIC
National and Kapodistrian University of Athens

Master Thesis

Epitaxial growth of Ga-polar GaN nanocolumns on Si(111) with AlN buffer layer

Επιταξιακή ανάπτυξη Ga-πολικών GaN nanocolumns σε υπόστρωμα πυριτίου(111) με ενδιάμεσο στρώμα AlN

Sandra Spanoudaki

Reg. Number: 201410
Department of Physics

supervised by
Prof. George Papaioannou Prof. Spiros Gardelis Prof. Angela Rizzi

co-supervisor
Dr. Joerg Malindretos

Athens
13th July 2016

Περίληψη

Στην διπλωματική αυτή εργασία μελετάται η ανάπτυξη Ga-πολικών GaN nanocolumns με την μέθοδο μοριακής επιταξίας δέσμης. Η εργασία χωρίζεται σε δύο μέρη.

Στο Μέρος Ι, γίνεται μία μικρή εισαγωγή στα θεωρητικά στοιχεία που είναι απαραίτητα ώστε να γίνει κατανοητή η εργασία. Περιλαμβάνει εισαγωγή στις πειραματικές μεθόδους που χρησιμοποιήθηκαν, μία εισαγωγή στα υλικά που μελετήθηκαν, και ένα προτεινόμενο μονοπάτι προς την επίτευξη των έλτιστων αποτελεσμάτων.

Στο Μέρος ΙΙ παρουσιάζονται τα αποτελέσματα της μελέτης εναπόθεσης λεπτών υμενίων άμορφου νιτριδίου του πυριτίου με την μέθοδο της χημικής εναπόθεσης με χρήση πλάσματος (PECVD), η ετεροεπιταξιά στρώματος AlN σε υπόστρωμα πυριτίου(111), και τέλος η ανάπτυξη GaN nanocolumns σε προεπιλεγμένες περιοχές. Ο δρόμος προς την βέλτιστη ανάπτυξη θα παρουσιαστεί.

Abstract

This thesis deals with the position-controlled selective area growth of Ga-polar nanocolumns by molecular beam epitaxy. The thesis is divided into two parts.

Part I reviews the theoretical background which is necessary for the understanding of this work. It consists of an introduction to the experimental techniques used in this work, an introduction to the materials studied and a suggested path towards optimal results.

Part II presents results on the study of the deposition of amorphous silicon nitride thin films by plasma-enhanced chemical vapor deposition, the heteroepitaxy of AlN buffer layer on Si(111), and finally the selective area growth of GaN nanocolumns. The route towards the optimization of the above steps will be presented.

An outlook of the thesis is following the above two parts, which summarizes the main achievements and conclusions of this research. Based on the results of this thesis, suggestions for future research on selective area growth of GaN nanocolumns by molecular beam epitaxy will by presented.

Contents

List of Figures

Introduction

GaN belongs to the group of III-nitrides and is considered one of the most important semiconductors after Si. Other important binary compounds of this group are InN and AlN, as well as their ternary and quaternary alloys ($In_xGa_{1-x}N$, $Al_yGa_{1-y}N$). Their bandgap is direct and is 6.015, 3.4 and 0.7 eV for AlN, GaN and InN respectively at room temperature. The astonishing property this group displays, is that it theoretically allows to tailor the fundamental band gap from the near infra-red (InN) to the far ultraviolet (AlN) (Fig. 1). Along with the wide band gap of GaN and AlN, which serves in high power applications, a variety of GaN based applications emerge when combining III-nitrides: photovoltaics, full visible spectrum LEDs, blue and green LDs for projectors (InGaN), ultraviolet LDs for photolithography, chemical analysis, medical and environmental applications [15], [40].

GaN-based high-efficiency LEDs have increasingly become a viable light source for illumination applications, such as automotive headlights, interior/exterior lighting and full color displays. It was in the early 1990s that Shuji Nakamura [29] developed a method of growing thin GaN layers on sapphire substrates and up to now, these have been the foundation of high-brightness blue LEDs (Fig. 2). GaN LEDs are grown on GaN templates mostly, on sapphire or silicon carbide and even though they give great results on the epitaxial growth of GaN, they are very expensive for commercial application. The solution to this is the integration of silicon as a substrate. The attempt to integrate III-V compound photonics into microelectronic circuits based on silicon, is a promiscuous attempt towards low-cost high performance optical systems.

Higher efficiencies can be achieved with single photon sources [31], [7], [9], [1], [23]. To reach a high efficiency, a high quality factor and low-mode volume is required, leading to the use of tapered photonic waveguides i.e nanowire taper waveguides, which leads to the replacement of layers by nanowires with embedded quantum dots. The advantage of the nanowire taper is the good directionality of photon emission from the nanowire. The quantum dots preferably should be distributed one per individual wavequide, otherwise the overall light-extraction efficiency [7]. For this purpose, nanowires are

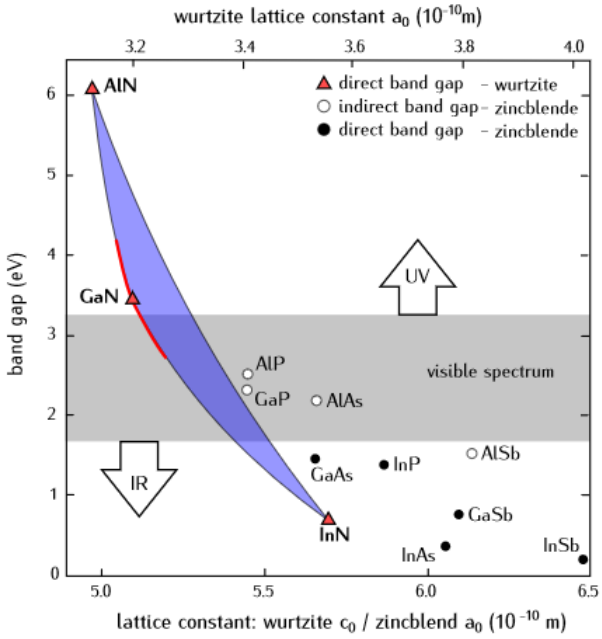

Figure 1: Band gaps of III-V compound semiconductors over lattice constants [5].

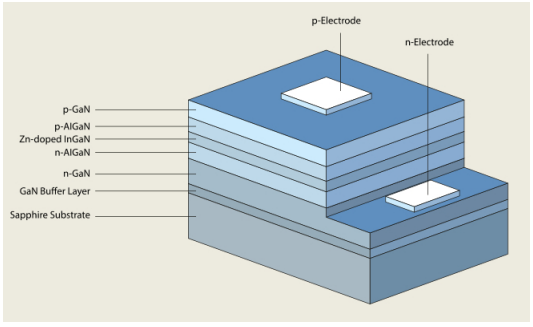

Figure 2: Structure of a blue LED with a InGaN/AlGaN double heterojunction [?]

selectively growing with the help of a patterned mask.

Selective area growth (SAG) is a catalyst-free epitaxial growth technique which combines a bottom up (epitaxy) and top-down technique (lithography) approach. The substrate is covered by a thin layer which is patterned by lithography. This layer, named the mask, is chemically inert and strongly prevents the nucleation of nanowires on it. The nucleation centres are the open areas where the mask has been removed. Selective epitaxy is used commonly in metal-organic phase epitaxy (MOVPE), including the case of GaN

nanowires, with SiO_x and SiN_x masks giving good selectivity for trimethyl gallium and trimethyl indium [20], [11] in SAG MOVPE. It has been evidenced that growth of GaN nanowires by MOVPE produces material with yellow luminescence, probably to carbon contamination. On the other hand, molecular beam epitaxy (MBE) process produces high quality, without contamination, materials. A problem that rises in MBE of GaN nanocolumns, is that the gallium tends to nucleates on the surface of masks, leading to the use of high temperatures to promote the Ga evaporation from the surface, while incorporating to the open areas. This requires a material with good thermal stability in the growth temperatures of GaN nanocolumns. Titanium and molybdenum masks, commonly used for the GaN SAG epitaxy have their upper limit to 800^oC. For higher temperatures they decompose, while at 800^oC they demonstrate parasitic nucleation. The parasitic nucleation, limits the studies in the competitive regime, which holds for aperture pitches smaller than twice the Ga adatom diffusion length on the substrate ($p<2\lambda_f$). In this regime, the ordered nucleation sites, imposed by SAG, are competitive for the Ga adatoms from the surface. The competitive regime introduces another parameter that one should be taking into account, the filing factor. The filling factor is lowering the direct flux by the percentage that gives the free space between divided by the whole space. This introduces the effective flux into the system. By increasing the substrate temperature, the Ga evaporation is enhanced, resulting in no contribution of the Ga adatoms due to diffusion to the nucleation. In this work, SiN_x is tested as an alternative to molybdenum and titanium, and it will be tested for its stability to high temperatures.

MOCVD has shown that nucleation of GaN layers directly on Si substrate is suppressed, due to the thin SiN_x layer formation during nitridation, that acts as inert layer at this temperatures [24]. To enable the epitaxy, the use of a buffer layer is a well-known approach. AlN has a quite large mismatch with Si (111) (+19.3%). Despite this mlarge misfit, it appears that the interface between (0001)AlN and Si(111) is completely abrupt with a coherent epitaxial relationship. A strain free AlN layer (complete relaxation down to 0.2%) occurs within one bilayer [24],[4], promising a good quality buffer layer for the nucleation of GaN nanocolumns.

The aim of this work is the selective area growth of GaN nanocolumns by molecular beam epitaxy on silicon. In our approach, AlN will be epitaxially grown on silicon as a buffer layer, while the mask will be a thin film of SiN_x deposited by plasma enhanced chemical vapor deposition (PECVD).

Part I

Theoretical Background

Chapter 1

Molecular Beam Epitaxy

1.1 Introduction to molecular beam epitaxy

Molecular Beam Epitaxy (MBE) is a technique for growing thin epitaxial structures. It was invented in the late 1960s by J. R. Arthur and Alfred Y. Cho. Since then, molecular beam epitaxy has experienced a tremendous development. MBE can be employed for the growth of group IV, III-V and II-VI semiconductors, metals, magnetic materials, nitrides, oxides and fluorides using solid and gaseous as well as metal-organic sources. By MBE several topics can be studied. To name a few, the investigation of the interfaces between epitaxially grown layers is possible by MBE, the amount of strain that is induced during hetero-epitaxy, as a result of the lattice mismatch, can be calculated, and moreover, fundamental studies can be performed, for instance on growth mechanisms.

In ultra high vacuum (UHV) environment, a thin film crystallizes through reactions of atoms that arrive in the form of beams on the surface of a substrate, which is maintained at elevated temperatures. The substrate acts as a seed crystal, and the deposited film may lock into one or more crystallographic orientations with respect to the substrate crystal. If the overlayer either forms a random orientation with respect to the substrate or does not form an ordered overlayer, it is termed non-epitaxial growth. If an epitaxial film is deposited on a substrate of the same composition, the process is called homoepitaxy; otherwise it is called heteroepitaxy. The growth rates are as low as one monolayer per second. Due to the technological difficulties regarding the UHV, MBE is not preferred in device production and instead, many epitaxial devices are fabricated by metal-organic vapor phase epitaxy (MOVPE). Some of the advantages of the MBE are that it provides the ability to control with precise the thickness of a layer, and compared to other

growth techniques, no complicated chemical reactions and gas flow dynamics take place at the substrate surface, which makes it easier the UHV environment in the growth chamber allows the application of various in-situ experimental techniques to study the processes governing crystal growth. At the same time, these measurements can be used to implement real-time feedback loops for growth control.

The essential parts of a MBE system are shown in fig. 1.1. The molecular beams are generated from liquid phase sources which are carried in Knudsen cells, when they are heated up at sufficiently high temperatures. The flux generated, is depended of the Knudsen cell geometry, the cell temperature and the equilibrium vapor pressure of the source material. The cells can be shut mechanically to turn the beams on and off, and they are heated up by filaments. For pressures below 10^{-5} mbar, the mean free path of the atoms evaporated from the cells is larger than the distance between the source and the substrate (≈30-50 cm), and subsequently the atoms form beams. Reactive nitrogen is supplied by excitation under plasma conditions. The plasma is excited by high fixed radio frequency field and variable power. The pure molecular nitrogen is kept into a gas bottle from where it flows to the crucible. The crucible is equipped with a perforated plate that separates partially the nitrogen from the growth chamber. The gas flow is regulated by a mass flow controller. Specific power and nitrogen flow conditions produce different types of reactive nitrogen. The substrate temperature is measured by a thermocouple and pyrometer.

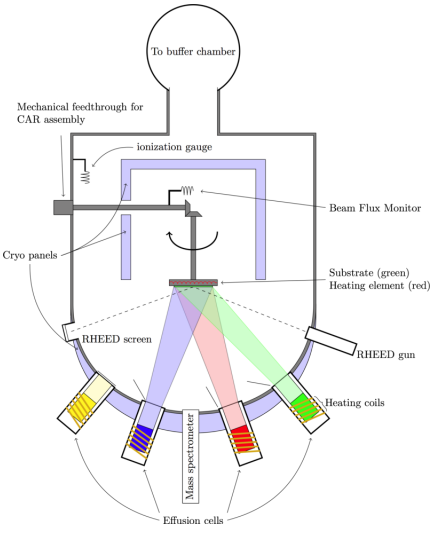

Figure 1.1: Layout representation of the reactor chamber of an MBE system [5]

The ultrahigh vacuum (UHV) pressures in the 10^{-10} mbar range are reached by ion getter pumps. Their role is to remove noble gases, which can act as impurity layers making the surface inert to the reactive gases of the experiment. Ultra high vacuum conditions are ensuring that, the time needed for these residual gases inside the reactor chamber to deposit one monolayer on the surface, is excessively larger than the time needed for a deposition of a monolayer from the molecular beams (10^5 times larger). For the calculations someone can refer to the book of Herman and Sitter [27]. During growth, a cryopump operating with liquid helium maintains the UHV. The increase of the pressure during growth is a result of the heat load from the effusion cells and the substrate [27] or the presence of nitrogen.

The UHV in the reactor chamber is maintained constantly. This is possible through a three chamber set up that build up the MBE. The first chamber, called load lock, is kept in pressures below 10^{-7} mbar. There the samples are heated up to reduce contaminations and moisture. The second chamber - the buffer chamber - is maintained in pressures below 10^{-9} mbar and there, the samples are heated again up until they are finally transferred into the growth chamber with base pressure of 10^{-10} mbar.

The atoms that evaporate from the effusion cell and impinge on the substrate surface can be treated as ideal gas under ultra high vacuum conditions. Hence, it holds that $p_v V = N k_B T_v$, where p_v is the vapor pressure inside the effusion cell, k_B is the Boltzmann constant and T_v the absolute temperature of the vapor. Pressure is related to the flux of atoms impinging on the unit surface area, by [27]:

$$F = \frac{p_v}{\sqrt{2\pi m k T_v}}$$

Hereby, measuring the cell temperature we can relate it to the pressure of the vapor which is proprortional to the flux.

1.2 Surface processes during MBE growth

When the impinging atoms reach the surface, they adsorb. Adsorption bounds weakly the atoms on the surface, making them easy to diffuse due to temperature gradient. After they reach the surface, the atoms diffuse on the surface and they nucleate, incorporate or desorb (Fig. 1.2). When the atoms gain enough thermal energy they leave the surface, and the rate of desorption increases exponentially with temperature [5]. At higher temperatures also, they possibly decompose.

Three modes of crystal growth exist: the layer-by-layer or Frank-van de Merwe mode, the island or Volmer-Weber mode, and the mix of the two, layer plus island or Stranski-Krastanov mode. The surface chemical potential determines which of those mode will be established. Markov proposed the following model for the layer chemical potential per atoms:

$$\mu(n) = \mu_\infty + [\varphi_\alpha - \acute{\varphi_\alpha}(n) + \epsilon_d(n) + \epsilon_e(n)] \tag{1.1}$$

where μ_∞ is the bulk chemical potential, φ_α the desorption energy of an adatom from a wetting layer, $\acute{\varphi_\alpha}$(n) the desorption energy of an adatom from the substrate, $\epsilon_d(n)$ the misfit dislocation energy per atom, and $\epsilon_e(n)$.

In the limit of small strains, $\epsilon_e(n) \ll \mu_\infty$ and the criterion of depends on the derivative $\frac{d\mu}{d\nu}$.

In the island mode (VM mode), small clusters nucleate on the substrate and then grow into islands because the adatom cohesive force is stronger that the surface adhesive force. This mode holds for $\frac{d\mu}{d\nu} > 0$ and it can also be a result of slow diffusion. In the layer-by-layer mode (FM mode), the surface adhesive force is stronger than the adatome cohesive force. The atoms are strongly bound to the substrate than to each other and the atoms condense to form a complete monolayer, until the second layer start to cover the first. The binding energy decreases from layer to layer monotonically and the derivative $\frac{d\mu}{d\nu}$ is negative. The VM mode is This mode is observed in systems of metals growing on insulators, whereas the FM mode is observed in the case of adsorbed gases, in some metal-metal systems and in semiconductor growth conditions and it can be a result of fast diffusion [27]. The intermediate condition includes the formation initially of some monolayers of the atoms and on top of them the formation of island if the energetics promote it. For instance if non trivial amounts of strain energy accumulate in the deposited layers during the layer-by-layer mode, at a critical thickness, this strain induces a sign reversal in the chemical potential, leading to a switch in the growth mode[28].

Growth is a non equilibrium process. If a vapor and a solid are in equilibrium, there will bw no effective mass transport, hence no growth. In the kinetic approach to describe the way of the system to equilibrium, the reaction are explained through activation barriers and via growth rates. The adsorbed atoms are weakly bound on the surface. The physical adsorption on the surface, depends on the arrival rate, interaction between different elements, availability of adsorption sites and activation barriers. The resulting adsorption rate can be characterized by the deposition rate of the impinging atoms and the sticking coefficient, which is the ration of the impinging to adsorbed atoms.[5]. Incorporation is the chemical bonding between the envolved to the growth precess atoms. In the case of GaN, the reaction of liquid gallium to gaseous nitrogen is more favored under MBE conditions compared to solid GaN , however, the kinetic barrier can be overcome for the reaction of Ga with a variety of nitrogen atomic species and therefore from GaN. The incorporation rate determines the growth rate. Keeping the nitrogen flux constant, the dependence of the growth rate with over the metal flux, give the stoichiometric point of the the growth (metal/N=1) as well the metal-rich and nitogen-rich regimes. For low metal-fluxes, the incorporation rate increases with metal flux, meaning that any additional metal atom find a nitrogen atom to incorporate. Subsequently, the growth rate increases. This is called the nitrogen-rich regime, because there is an onersupply of nitrogen

and metal/N<1. At high metal-fluxes, all nitrogen atoms already incorporated, resulting in a constant growth rate. This is called metal-rich regime and the plot growth time over metal-flux provides the surface stoichiometry (fig. 1.3). This plot can be derved for every III-N compound.

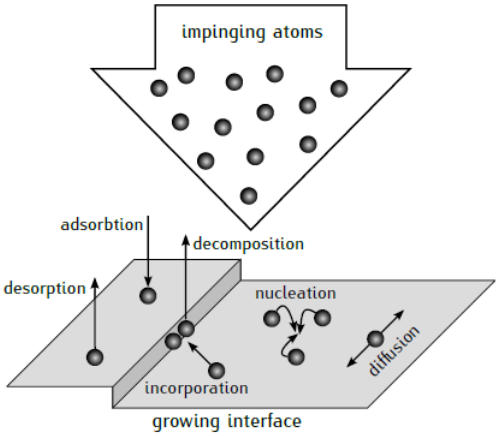

Figure 1.2: Surface processes during MBE growth: adsorption, diffusion, followed by incorporation, nucleation, or decomposition

Desorption occurs when the atoms gain enough thermal energy to leave the surface. The desorption rate increases exponentially with the surface temperature. It depends on the bond strength of the adsorbed atom and the surface, the activation energy for the desorption. The activation energy for the nitrogen is much higher and for Ga, because it can only desorb as a ground state N_2, as the other sates require higher energies than those supplied thermally by the substrate. This process require the diffusion and bonding od two N atoms on the surface and therefore this process is also depended on the surface diffusion, whereas metal atoms desorb directly. Another possible path for desorption of nitrogen is to bond an adsorbed with an incorporated atoms, and this process is assisted by increased temperature. Finally, at high temperatures, a high amount of nitrogen in the impinging nitrogen flux results in the decomposition of the III-V compound.

For high quality semiconductor growth, a general rule assigns as optimal growth temperature the 1/2 or 1/3 of the melting point temperature of the semiconductor compound. The nitrogen equilibrium vapor pressure over substrate temperature indicates whether the III-V material can be grown at the optimal temperature T_{opt} under the MBE pressure of 10^{-5}mbar. As it can be seen in Fig. 1.4, in the typical pressure of 10^{-5}mbar of the MBE, only AlN can be grown at T_{opt}. For this reason, growth on lower temperatures is

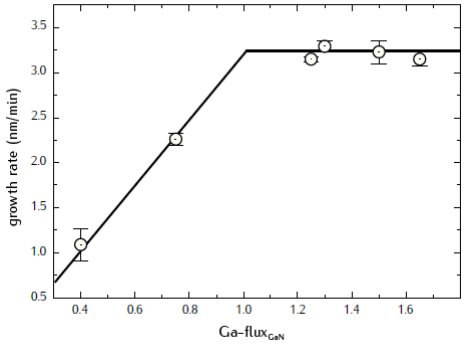

Figure 1.3: Growth rate of GaN depending on Ga flux, normalized to GaN stoichiometry. The saturated region on the right is the Ga-rich regime, the N-rich regime holds for increasing growth rates, and the intermediate point is the stoichiometric (Ga/N=1) [5]

required, in order to avoid decomposition [5].

All the surface processes described above are highly depended on the surface diffusion. Longer diffusion length of adatoms result in smooth layers , whereas short produce rough structures. The diffusion length is given by the diffusion coefficient and the time the adatom stays on the surface. The diffusion coefficient increases exponentially with temperature and the residence time depends on the surface processes. Thus the desorption rate limits the diffusion length at high temperatures. If the growth rate increases, the time till incorporation shortens, resulting in rougher surfaces. Hence, the diffusion length is limited by desorption in higher temperatures and by incorporation in low temperatures, and is depended on the Ga/N ratio.

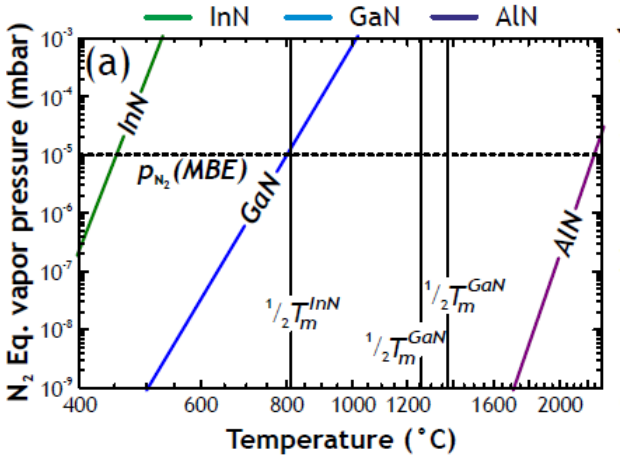

Figure 1.4: Thermal stability of InN, GaN, AlN. Under MBE pressures, only AlN can grow at the optimal growth temperature [5].

Chapter 2

Reflection high-energy electron diffraction

The Reflection High-energy diffraction method provides an *in situ* characterization tool in MBE. RHEED is a method based on diffraction of high-energy electrons from a clean and well-ordered surface in ultra high vaccum. Electrons with energy in the range of 10 keV, probe the sample with a small incident angle (typically $<3^o$) and they scatter elastically penetrating only the first few atomic layers, allowing a real-time surface monitoring during growth. The incident electron beam is diffracted from the surface and the image of it on the phosphor screen is referred to as reflection spot. The informations one can extract from the intensity of this spot is the roughness of the surface, the strain that the grown layer acquires or not relatively to the substrate, and the period of the monolayer growth measuring the periodic oscillation the specular beam spot undergoes.

In the ideal case of electrons diffracting from the first atomic layer of a flat and ordered surface, the 3 dimensional lattice points, in the reciprocal space, degenerate into parallel infinite rods. A schematic representation of the rods formation is given in fig. 2.1. These infinite rods have a finite thickness due to thermal vibrations and imperfections, while further broaden of their thickness is caused by the atomic steps created by islands on the surface [5].

In the kinematic scattering theory, the possible reflections are given by the condition that the incident wavevectors $\boldsymbol{k}_0$ and the diffracted $\boldsymbol{k}'$ differ by a reciprocal-lattice vector $\boldsymbol{G}$:

$$\boldsymbol{k}_0 - \boldsymbol{k}' = \boldsymbol{G} \tag{2.1}$$

For elastic scattering, where $\|\boldsymbol{k}_0\|=\|\boldsymbol{k}'\|$, this condition is the origin of the Ewald sphere in reciprocal space, where the tip of $\boldsymbol{k}_0$ is attached to a

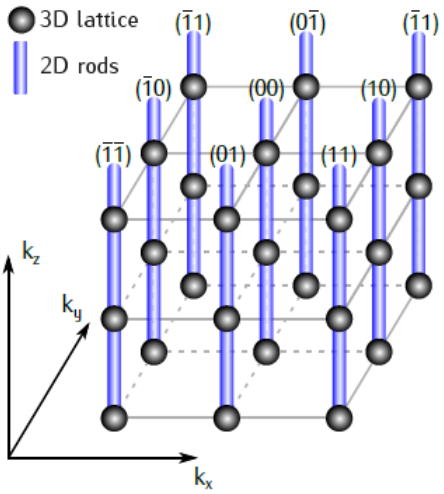

Figure 2.1: Degeneration of diffraction spots into rods for the the 2D condition [5]

reciprocal-lattice point and the sphere around the origin of $\boldsymbol{k}_0$ with radius $\|\boldsymbol{k}_0\|$ defines the Ewald sphere. Reflections can occur for every $\boldsymbol{k}'$ that connects the origin of the sphere and a reciprocal lattice point on the sphere. The magnitude of the wavevector for high-energy electrons are given by:

$$k_0 = 1/\hbar\sqrt{2m_0E + E^2/c^2}$$

For 14keV electrons, which is used in this work, k_0 is 630 nm^{-1}. This means that the Ewald sphere is large with radius about 31 times larger than the reciprocal-lattice unit of AlN ($2\pi/a$, where a is the in-plane lattice constant, equal to 0,311nm at 300^{o}K), producing an almost planarcut through the first few Brillouin zones of the reciprocal lattice. The Ewald sphere construction and the diffraction geometry are shown in fig 2.2, where the reflections occur on the Laue circles of radius L_n centered at H.

In a 2D surface, the intersection of the lattice rods with the Ewald sphere result in points in a RHEED pattern. In reality however, the broadening of the lattice rods as well as the shell of the Ewald sphere created by the not fully monochrome electron beam, adding the finite size of the crystal, result in a larger cross section of the rods and the Ewald sphere. In the case of a rough surface, the lattice rods form segments according to the 3D reciprocal lattice. A spotty RHEED pattern indicating rough surface is shown in fig. 2.4. Note that the segments of a 3D surface are broader, resulting in bigger overlap with the Ewald sphere, thus broader RHEED pattern. A streaky

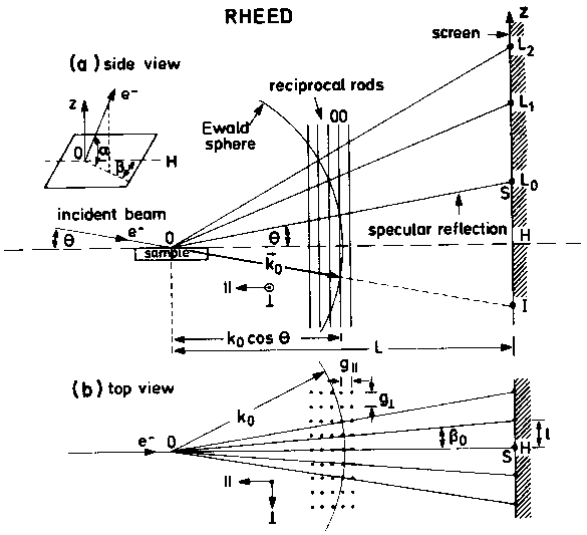

Figure 2.2: Diffraction geometry of RHEED. adapted from Braun [?]

RHEED pattern of a smooth surface is shown in fig. 2.3

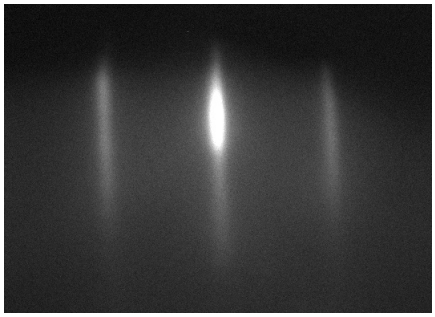

Figure 2.3: Streaky RHEED pattern, as a result of a smooth surface, the specular spot is the brighter at the center

Finally, during 2D nucleation growth, 2D nuclei form on the surface and grow laterally until they merge. At the end of the monolayer coverage from the nuclei, the process repeats again. The above describe the layer by layer growth mode, and makes the RHEED intensity to oscillate periodically. When the monolayer is covered, the intensity is maximal. The intensity drops while the nuclei cover the surface and gets the minimal value for half covered layer. From that point, intensity recovers, creating the periodic oscillations. A schematic of the RHEED oscillations is given in fig. 2.5.

The number of oscillations in time, determine the time needed to build a monolayer, which leads to an estimation of the epitaxial growth rate. In the

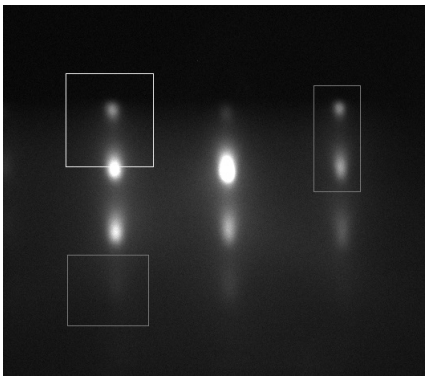

Figure 2.4: Spotty RHEED pattern, indicative of a rough (3D) surface

case of a growth consisting of islands formation, no oscillations are observed and this happens primarily in the case of heteroepitaxy that might appear a disordered interface due to large lattice mismatch, as in the case of AlN on Si that concerns this work.

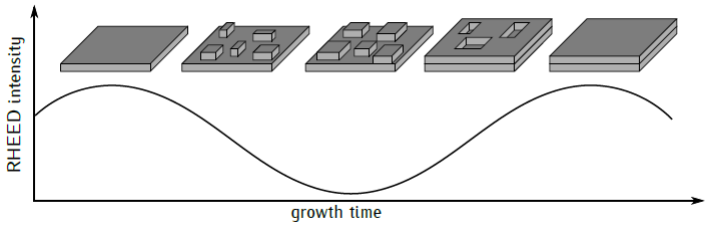

Figure 2.5: Oscillations of RHEED intensity over time due to monolayer coverage by the nuclei [5]

Chapter 3

Silicon

3.1 Si properties

Silicon is the most perfected and least expensive substrate available in sizes up to 300mm. It is thermally stable under GaN epitaxy temperatures and, Even though the epitaxy of Wz GaN and AlN grown on Si(111) is highly defective, the incentives for using Si substrates are high, and good progress has been done to reduce the defect density.

Si has a diamond-lattice structure, with lattice constant of 0.543 nm at 300^o and can be thought of as two fcc sublattices interpenetrating, with one sublattice displaced from the other by one quarter of the distance along a body diagonal of the cube. Each atom in the lattice is surrounded by for equidistant nearest neighbours that lie at the corners of a tetrahedron. Figure 3.1 illustrates the crystal structure of silicon. The red is the (111) lattice plane and at (b) is shown the top view of the (111) oriented silicon surface. Cleavage along the (111) orientation provides the proper substrate orientation for the epitaxy of wurtzite structures along the [0001] direction. It belongs to the group of semiconductors with an indirect band-gap of 1.12 eV at 300^oK and it has a melting point of 1414^oC.

3.2 Si as a substrate for epitaxy

Any kind of contaminations on the surface of the substrate, such as moisture, carbon, oxygen will constitute source of additional dislocations during epitaxy, which will follow the growth directions and do not annihilate or leave the crystal at its boundaries. For this reason, the dislocation density of the substrate must be minimal, as it determines the smallest possible number of dislocations for a growth structure. The above argument, indicates the

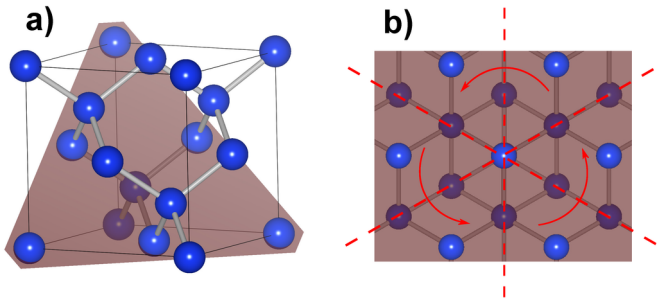

Figure 3.1: Crystal structure of silicon. (a) Unit cell with (111) oriented lattice plane marked with red and the top view (b) of the (111) oriented silicon surface. Wafers cut along this orientation, provide suitable substrate for the epitaxy of Wurtzite structures along the [0001] direction. Picture taken by Schriever Clemens et al.

importance of the pretreatment of the substrate prior growth. Except from the standard cleaning process of the substrates, which consists of ultrasonic baths in aceton, methanol and di-ionized water, and the further heating up of them in the load-lock and buffer chamber of the MBE, one more step is added for Si(111), by heating it up to 1080^{o}C and letting it cool down slowly until 990^{o}C where the 7x7 surface reconstruction appears, indicating successful cleaning of the Si(111).

3.3 Si(7x7) - surface reconstruction

Surface reconstruction refers to the process by which, atoms at the surface of a crystal assume a different structure than that of the bulk. It is important to identify these rearrangements, especially when the reconstructed surface is an interface, because this new configuration is providing the sites, for the atoms of the following layer, to bond.

In an ideal infinite crystal, the equilibrium position of each individual atom is determined by the forces exerted by all the other atoms in the crystal, resulting in a periodic structure. If a surface is introduced to the system by terminating the crystal along a given plane, then these forces are altered, changing the equilibrium positions of the remaining atoms. This is noticeable for the atoms at and near the surface plane, as they now only experience inter-atomic forces from one direction. This imbalance results in the atoms near the surface assuming positions with different spacing and/or symmetry from the bulk atoms, creating a different surface structure. This change in equilibrium positions near the surface can be categorized as either a re-

laxation or a reconstruction. A reconstruction can also either conserve the total number of atoms in a layer or have a greater or lesser number than in the bulk. The relaxations and reconstructions considered above describe the ideal case of atomically clean surfaces in vacuum, in which the interaction with another medium is not considered. However, reconstructions can also be induced or affected by the adsorption of other atoms onto the surface, as the interatomic forces are changed, and they are more extensive in chemisorption than physisorption.

Silicon exhibits several well-ordered reconstructions depending on temperature and on which crystal face is exposed. Cleavage of Si along the (111) surfaces at low temperatures results in a 2x1 reconstruction, while when heated above 400 ^{o}C this structure converts irreversibly to the more complicated 7x7 reconstruction. A disordered 1x1 structure is regained at temperatures above 830 ^{o}C, which can be converted back to the 7x7 reconstruction by slow cooling [12]. The 7x7 reconstruction is modeled according to a surface model with dimers, adatoms and stacking (DAS) faults that was proposed by Kunio Takayanagi in 1985. A unit cell with 7x7 reconstruction consists of an angle cavity and two triangular subcells separated by dimer chains. Each subcell contains 6 adatoms adsorbed on the crystal surface but not yet associated with the crystalline lattice. The atomic layer below the adatom layer in one of the subcells has a stacking fault orientation. The adequacy of this model was confirmed by multiple tests [36]. In Fig. 3.2 are shown scanning tunneling microscopy (STM) images of a Si(111)7x7 surface, along with the schematic representation. The yellow circles represent Si atoms, the red circles dimerized Si atoms and the blue, second layer Si rest-atoms. The elementary 7x7 cell is highlighted with a diamond. Half of the elementary cell with package defect is marked as FH (faulted half) and the half with no package defect marked as UH (unfaulted half). In the STM image of filled states (a), the half of the cell with package defect appears brighter than the other half. For further study of this topic, one can refer to the study of Takayanagi [36].

In this work, every sample had been outgased up tp 990 ^{o}C pyrometer temperature where the 1x1 surface reconstruction appears and then was being cooled slowly down passing to the 7x7 rearrangement. The transition took place at around 830 ^{o}C pyrometer temperature, in good agreement with previous works and literature. As it will be shown in chapter , the temperature of the substrate upon the start of nucleation is deterministic for the whole epitaxy, when the other parameters where kept "constant", and this is manifested by the surface roughness measured by atomic force microscopy (AFM). A possible reason for that will be discussed in the chapter 4 that

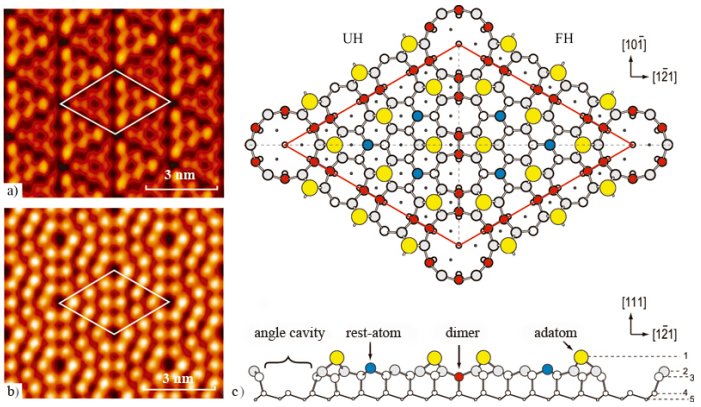

Figure 3.2: Atomically clean surface of Si(111)7x7. STM images of (a) filled and (b) unfilled electron states of surface; schematic representation of surface at (c) plan and side views [36].

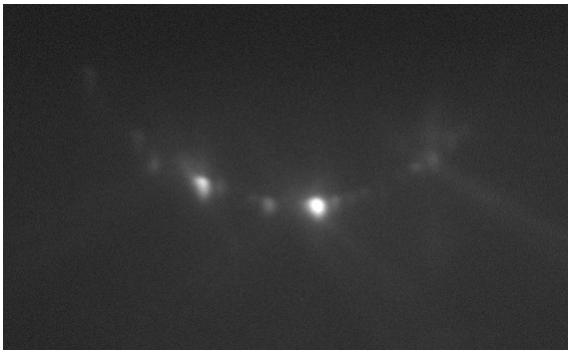

Figure 3.3: RHEED on atomically clean surface of Si(111)7x7.

follows.

Chapter 4

AlN buffer layer

4.1 General properties of aluminium nitride (AlN)

AlN is a direct bandgap semiconductor with a bandgap of 6.2 eV at room temperature and still considered to be semiconductor. AlN has wurtzitic and zinc blende polytypes with the latter being very unstable and hard to synthesize. It has a melting point of 2200°C and his lattice constant are a_0=0.3112 nm and c_0=0.4982 nm at room temperature.

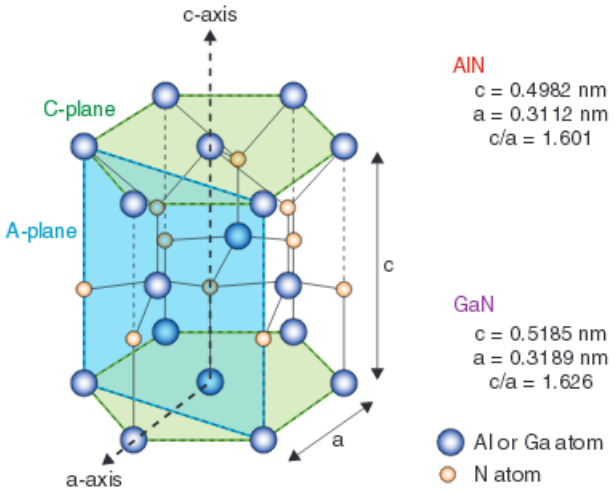

Figure 4.1: Wurtzite strucure of AlN and GaN [37]

4.2 Growth of AlN

AlN is used as a buffer layer in the case of GaN NCs grown on Si, because otherwise the formation of a SiN_x layer on the Si surface would prohibit the selectivity mechanism.

The most popular method used to obtain high quality AlN layers is metal-organic vapor phase epitaxy. Molecular beam epitaxy has advantages of *in-situ* monitoring and a relatively low growth temperature. AlN has been reported to be thermodynamically stable under MBE conditions and elevated temperatures can be used up to around 1500^oC without decomposition issues.

The diagram of the growth rate over metal-flux, for constant nitrogen flux, divides the growth of the III-nitride compound into two regimes. In particular, keeping the nitrogen flux fixed, if the aluminium flux is low, every aluminium surface. From that point, if the aluminium flux starts to increase, the growth rate will keep increasing due larger number of adatoms available for incorporation. This is called the nitrogen-rich regime and for the fluxes holds that Al/N<1. The increase of the growth rate is continuing until the the saturation of it in a constant value. When this regime is reached, the growth rate doesn't change over larger aluminium fluxes, because all the nitrogen atoms are incorporated and there are no more N-adatoms to contribute to growth. This regime is the aluminium-rich regime where Al/N>1. The crossover from the one regime to the other, defines the stoichiometric point where Al/N=1 and is the point where the layer-by-layer growth takes place, for the specific substrate temperature, those experiments take place. The stoichiometric point can also be detected with the RHEED oscillations. As explained in section 2, layer-by-layer growth results in oscillations of the RHEED intensity. Slightly N-rich or Al-rich conditions give again oscillations but with different behaviours, which are well understood, and can help us to modulate the aluminium flux until we reach stoichiometry. This technique is very useful to determine the stoichiometric conditions (Al/N=1) and subsequently the growth rate and the two regimes- nitrogen rich and aluminium rich. However, the success of this technique strongly requires growth on substrate of the same material. In the case of AlN, the method is to expose a (0001)sapphire wafer to a nitrogen plasma for about 45 min. [10] [30], which will convert a thin sapphire layer into AlN under tensile stress with respect to the sapphire substrate. In the case of a foreign substrate, one cannot observe oscillations. It has been reported by several works that optimal growth for AlN is for Al/N ratio slightly above 1, and one can go by trial and error to determine which growth conditions lead to the slightly Al-rich regime, but undetected growth system changes, such as thermal deviations of the substrate or of the effusion cells, make it difficult to maintain the same conditions

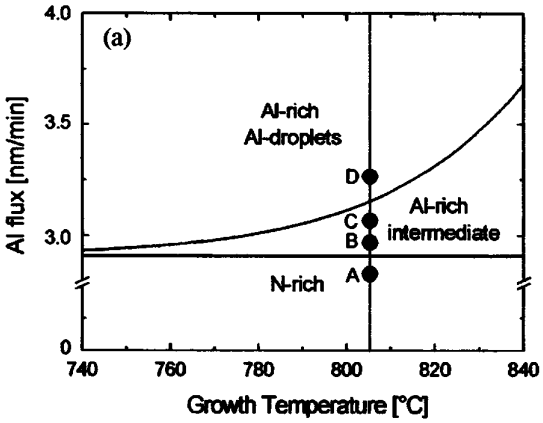

Figure 4.2: Growth diagram for AlN giving Al fluxes and growth temperatures for the N-rich, intermediate and Al-droplet regimes at a constant N flux of 2.9 nm/min. as reported be Koblmueller et al. [13]

over the growths. Moreover, it has been reported [13] the growth window to obtain an Al-droplet-free surface is too narrow to be well controlled in the usual growth temperatures (around 780^{o}C). The reason for that is that at these low temperatures (700-800 ^{o}C) Al adatoms have low re-evaporization rate and it is difficult to avoid the formation of Al droplets. Fig. 4.2 shows the growth diagram of AlN by MBE. Similar to GaN, most of the epitaxy is performed under the intermediate regime. As it can be seen in Fig. 4.2, the growth window broadens with increasing growth temperature. Pan et *al.* [30] have reported on Al droplet-free surface at 950 ^{o}C based on the broadening of the intermediate-regime windoew. Under these high temperatures, the droplet-free surface occurs due to the enhanced re-evaporization rate and migration ability of Al adatoms.

However, a reproducible technique has not been found yet. Recently, Burnham et *al* introduced the metal modulation epitaxy (MME) technique, of which further information can be found in the parer given [6]. In this work, the idea of consuming the aluminium droplets after the epitaxy was used, by nitridation during cooling down, which gave good surface morphologies, without droplets. The epitaxy was taking place in aluminium rich conditions that without nitridation is known to result in droplets.

Regarding the interface between the two materials,in principle, when two crystal lattices have a large mismatch (>13%) a three dimensional growth takes place, by the formation of columnar film structure, and a high defect density is expected to generate due to the strain energy unless the entire misfit is relaxed at the interface. In the case of Al and Si, their lattice

mismatch is large (+19.3%). However, many research has been done on the interface of (0001)AlN and (111)Si, and a planar interface is observed between the diamond cubic and the wurtzite lattice structures. The continuity of the lattice planes across the interface indicates coherent epitaxy. Transmission electron microscopy (TEM) shows a direct bonding between AlN and Si groups without the presence of a SiN_x layer (Fig. 4.3). This suggests that the substrate is protected from pre-growth exposure to plasma. In a similar work, Liu et *al* reported that an initial Al exposure (10s) was necessary during MOVPE, otherwise the film morphology and crystallinity was very poor [24], however, the Al layer was not detected in *ex-situ* analysis. The strain that results due to the large lattice mismatch, is relieved by the introduction of a periodic array of misfit dislocations as can be seen in figures 4.3,4.4. The average separation is about 5.3 $\{1\text{-}100\}_{AlN}$ planes, which is equal to 4.3 $\{111\}_{Si}$ planes. Finally, a schematic of the misfit dislocations on the basal plane and in cross section is given in fig 4.5. The dislocation lines are along $\langle 11\text{-}20\rangle_{AlN}$ directions. The density of the dangling bonds due to the misfit dislocations can be calculated to be close to half that of the interface bonds. Such a high density of dangling bonds strongly influences tha atomic arrangement at the interface [24].

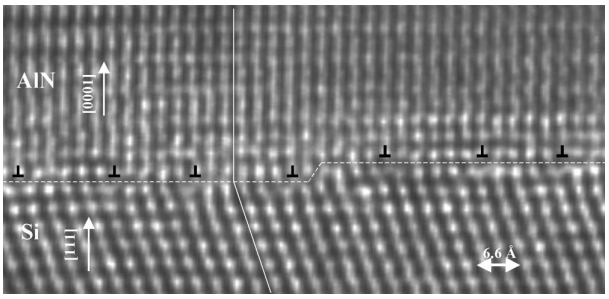

Figure 4.3: TEM image showing and abrupt Al(0001)/Si(111) interface, marked by the horizontal dashed line. Misfit dislocations are indicated by "⊥". The interface coherence is indicated by solid lines

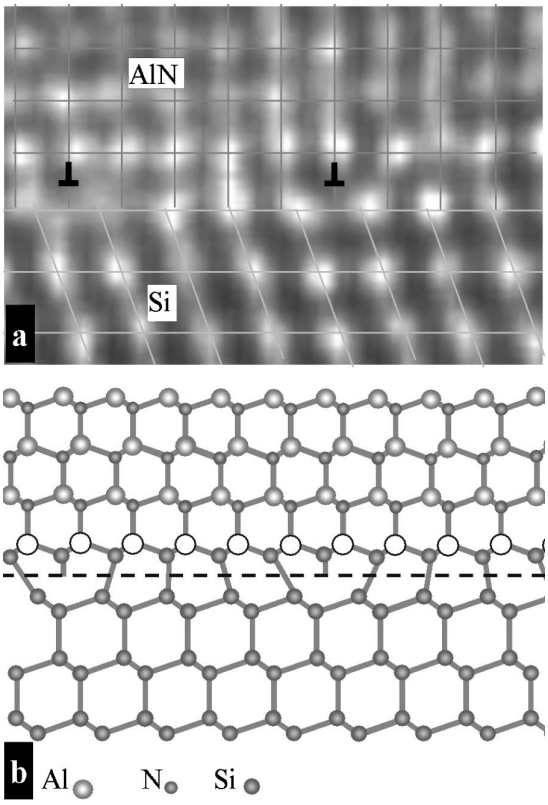

Figure 4.4: (a)Closer look at the atomic arrangement at the Al(0001)/Si(111) interface as resulted by TEM. Schematic of the atomic arrangement in cross section, as depicted by Liu et at [24]. Open circles could be N, Al, or Si.

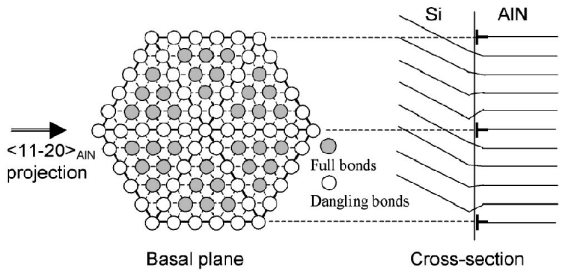

Figure 4.5: Misfit dislocations on the basal plane and in cross section. The density of dangling bonds on the basal plane is about one half the total number of interface bonds. Schematic by Liu et al. [24]

4.3 Importance of Si7x7 surface reconstruction during AlN grown on Si by MBE

As it has been reported above, despite the misfit of +19.3% between Si(111) and AlN(0001), a complete relaxation down to ∽0.2% occurs within one bilayer [3]. This fact indicates that epitaxy might occur directly on Si(111) in 2DG mode. The key to this achievement is the formation of the Si(111)-7x7 reconstruction surface. This Si(111)-7x7 surface has a complex atomic arrangement and the depth of the structure is of three monolayers deep. It has been suggested that this atomic arrangement favors the creation of a new material superstructure with a partial substitution of the substrate adatoms and restatoms by the adsorbed Al and N atoms of the nucleating layer. Subsequently, the arrangement of the initially adsorbed atoms establishes the regular array of the surface supercells which is responsible for the 2DG of the epitaxial layer with its own lattice constant. This gives a sensible solution to the almost full AlN lattice constant relaxation in 1-2 monolayers from the hetero-interface according to Lebedev et *al.* t has been reported that no proper nucleation has been observed on the flat Si-1x1 surface. Hence, exist of the Si(111)-7x7 reconstruction surface must be highlighted as requisite condition for the 2DG AlN.

Bourret et *al.* studied further the existence of this supercell. Specifically, XRD measurements revealed that there is no sign of (7x7) silicon reconstruction or a periodic supercell described above. Diffuse scattering around 02-2 showed strong and anomalously wide-angle diffuse scattering around the Si diffraction peaks. For this observation, they suggested that the intermediate layer at the interface is completely disorganized giving the wide scattering and closely related to the substrate lattice (i.e, with the same periodicity). This could be interpreted by a layer composed of small patches of nearly

coincident AlN on Si (atoms close to the silicon lattice), but randomly dispersed on the surface. This also implies a low mobility of the AlN species on Si which inhibits any further rearrangement.

4.4 Polarity of AlN grown on Si(111)

For NC-based optoelectronic devices, the NC polarity is of great interest since it determines the direction of spontaneous and piezoelectric polarization. Furthermore, polarity plays important role when it comes for the incorporation of another component.

Not many reports on the polarity of SAG GaN nanocolumns exists. However, in the case of the SAG GaN NCs grown on Ga polar GaN templates, the polarity of the NCs has been found to be Ga-polar [39]. This suggests that the AlN should be Al terminated. Lebedev et al. have demonstrated, using X-ray photoelectron diffraction (XPD) and RHEED, that substrate temperature when the nucleation begins determines the polarity of the AlN grown layers. In particular, layers grown at low temperatures (700^{o}C)in the first place and then ramping up to 860-880^{o}C were found to be unipolar with N-face polarity. Layers grown with starting temperatures of 770-800^{o}C and then ramping up to higher temperatures were unipolar demonstrating Al-face polarity. For significantly higher starting temperatures (880-900^{o}C), the epitaxy had no acceptable surface quality (rms 5nm) and mixed polarity. However, to ensure the polarity of the AlN layer, further investigation should be done, which includes wet etching experiments. An identification of the polarity of the AlN and the GaN that follows, are the observations of the morphology of the GaN NC tip, which is pyramidal for the Ga-polar NC and c-plane ending for the N-polar NCs.

Chapter 5

Amorphous silicon nitride-PECVD

5.1 Introduction to PECVD

Silicon nitride (Si_3N_4) is a widely used material in semiconductor technology serving many roles, from passivation to insulation, mechanical protection, or capping layer during implantation.

In this work Si_3N_4 has been studied as an alternative to molybdenun (Mo) and titanium (Ti) metal masks that has been already studied until now. The problems that Si_3N_4 aims to solve or to optimize are to provide a better thermal stability, at high temperatures needed for growth, and less or absence of parasitic nucleation on the mask, namely good selectivity. Until now, selective area growth of GaN nanocolumns on metal masks (Mo,Ti) appears imperfect, because non negligible self organized nucleation on the mask limits the studies at the competitive regime.

Silicon nirtride is deposited in the form of an amorphous layer (SiN_x) using the plasma enhanced chemical vapor deposition (PECVD) techinique. In the following section this method the basic characteristics of this method will be described. Furthermore, a description of the chemical process that takes place during the deposition will be cited, which will guide someone to choose the right parameters for the process and optimise it.

PECVD is a chemical vapor deposition (CVD) method. CVD is a process to deposit high quality thin films from gas state (vapor) to solid state on a substrate, through the reaction of molecules or atoms, on the surface of a substrate. Plasma enhanced-CVD assists the plasma for the dissociation of the precursor gases. The advantage of PECVD is that the deposition takes place at lower temperaturess (250^oC-350^oC) than that of CVD (600^oC-800^oC), and

this is critical in the case of applications where high temperatures could damage the device being fabricated. The reason for this is that the plasma-kinetic energy causes much less heating and degradation of the substrate, in comparison to thermal CVD. The plasma is created by RF (alternating current) discharge between two parallel electrodes - a grounded electrode and an RF-energized electrode. Processing plasmas are typically operated at pressures of a few millitorr.

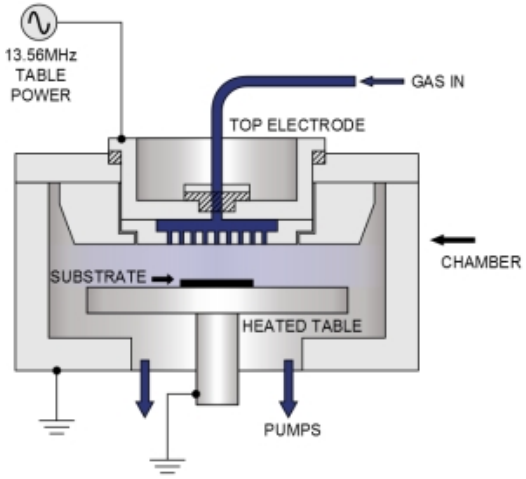

Figure 5.1: Schematic representation of a Plasma Enhanced Chemical Vapour Deposition reactor

When the plasma is initiated, few free electrons gain kinetic energy rapidly through the electric field, which they slowly lose through inelastic collisions. The inelastic collisions with the reactant gas molecules cause the latter to dissociate and ionize, producing secondary electrons. Two aspects of the procedure should be considered when studying the plasma discharge physics. At first, the gas-phase non equilibrium low-temperature chemical reactions that generate radical and ion reactive species in the plasma discharge, and subsequently, the flux and energy of these reactive species when they reach and strike the substrate.

The reactions during plasma are complex and not yet understood completely and occur during four steps. To start with, the primary electron-impact reactions between electron and reactant gases occur, to form ions and radical reactive species. Follows the transport of these reactive species from the plasma to the substrate comprising elastic and inelastic collisions in the plasma and sheath region. This step generates ions and radicals as well. These steps affect the uniformity, the density, the strain and the "impurity" incorporation. The third step is the absorption and/or reaction of

the reactive species. Finally, the reactive species and the reaction products incorporate into the deposited film or desorb. These last steps are the least known and studied due to their complexity and affect greately the surface morphology and the chemical composition of the film [34].

The RF plasma-generated reactions for SiN_x deposition, with E_D the dissociation energy are:

$$\begin{aligned} N_2 + e^- \rightarrow 2N + e^- \quad &, \quad E_D = 9.8 \text{ eV} \\ SiH_4 + e^- \rightarrow SiH_2 + H_2 + e^- \quad &, \quad E_D = 3.97 \text{ eV} \\ NH_3 + e^- \rightarrow NH_2 + H + e^- \quad &, \quad E_D = 4.6 \text{ eV} \end{aligned}$$

The stress control of the deposited film of SiN_x is feasible and of great importance. When too many atoms are packed into the film, the bond lengths are pushed shorter than normal. The film tries to relax back to its normal bond length, pushing outwards and forcing a convex "compressive stress" curvature of the wafer. The opposite happens when there are too few atoms per cm^3, which is the tensile stress condition. In this notation the predeposited silicon wafer is considered stress free. Many studies have been done on the nature of the stress of PECVD on Si test wafers. At 13.56 MHz, SiN_x films prepared from standard gas mixtures of SiH_4, NH_3, N_2 are typically tensile in nature. The addition of low frequency (1<MHz) component enhances the deposition and changes the stress to compressive [19]. Significant role play as well the SiH_4 flow rate, the $SiH_4 \backslash NH_3$ ratio, the pressure and the substrate temperature.

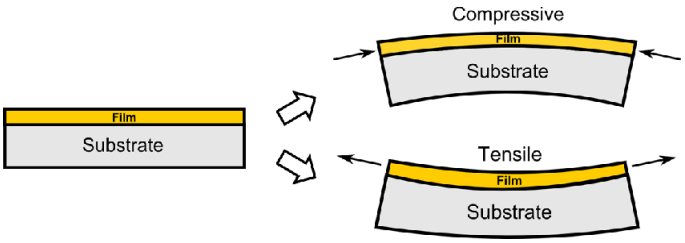

Figure 5.2: Original wafer on the right side, wafer shape after depositing compressive or tensile film

Almost all the SiH_4 in a typical discharge dissociates into SiH_n (n<4) even at extremely low densities [33]. With high NH_3 flow rate, essentially all of the SiH_4 is converted to tetra-aminosilane ($Si(NH_2)_4$) and triaminosilane ($Si(NH_2)_3$). These radicals do not react with the surface but adsorb on the surface with a low-sticking coefficient, and there they undergo chemical condensation towards stoichiometric Si_3N_4, with the elimination of ammonia,

which is evolved again into the plasma. To give an example of a possible reaction path in the case of $Si(NH_2)_4$:

$$SiH_4 + 4NH_3 \rightarrow Si(NH_2)_4 + 4H_2$$

$$3Si(NH_2)_4 \rightarrow Si_3N_4 + 8NH_3$$

The higher the substrate temperature , the further the second reaction proceeds, due to enhanced diffusion, generating tensile stress. On the other hand, low NH_3 flow rate will result in a Si-rich SiN_x layer, and the high silicon content yields a lower stress level. Furthermore, SiH and SiN generated radicals can lead to direct growth of solid Si_3H_4 film on the surface, through reaction with active nitrogen, as it has been reported after chemiluminescence experiments [2]. The following two reactions or their combination could take place :

$$6SiH + 8N \rightarrow 2Si_3NH_4 + 3H_2$$

$$3SiN + N \rightarrow Si_3H_4$$

If the power is enough to dissociate all the SiH_4 to SiH_n but not enough to dissociate all the N_2 to N, then some SiH_n may react with itself to form Si_2H_n by-products . This results in low deposition rates and Si-rich films [33]. The inactivated N_2 molecules do not react with SiH_n, and act as inert diluents. As the power is raised, $N_2 \rightarrow N$ dissociation increases, therefore both the deposition rate and N/Si ratio in the bulk of the film are expected to increase. Finally, for the role of hydrogen, the presence of it on the surface causes passivation against any adsorption due to formation of strong bond with the surface. This primary description is sufficient to first understand how to modulate and optimise the surface morphology of the deposited film.

5.2 Stress and deposition rate of PECVD SiN_x

The stress of the SiN_x deposition under plasma, has been well investigated by Iliescu et *al* [19]. Beginning from the RF power, the increased RF power leads to a higher electron density and therefore to a relatively larger population of higher-energy electrons. These high-energy electrons yield a higher ionization and dissociation rate, which consequently results in a higher deposition rate. High power also leads to more N^+ species and consequently results in increased incorporation of N bonding in the SiNx film. This results in compressive stress due to the volume expansion of the SiN_x film [19] which

compensates the tensile stress of the whole layer and leads to overall lower tensile stress. On the other hand, in the case of low power (20-80 W), it has been observed that deposition in HF mode generates a tensile stress of 120-150 MPa [19] and lower deposition rates. Whereas, LF mode at low power, in the range stated above impose high compressive stress in the range of -690 to -570 MPa, for increasing power from 20 W to 80 W. The explanation for this is that at high frequencies only the electrons follow the RF field while the ions are frozen in their place due to heavier mass. The crossover frequency at which ions start following the electric field is between 1-5MHz. Below that point, the ion-bombardment is significantly higher, which enhances chemical reactions but also causes low energy ion implantation that densifies the film and leads to a change of stress from tensile to compressive ([18], [19]). Hence, it is suggested that, for a thin film deposition in the thickness range of ten nanometres, low deposition rates should be used, and therefore low power. The continuous alteration of HF mode to LF mode seems to be of great importance to balance the residual stress and achieve layers with "zero residual stress". Finally, it has to be mentioned that to achieve a homogeneous layer in the case of mixed-frequencies mode, the thickness of the individual compressive or tensile layers must be as thin as possible leading back to the necessity of low deposition rates, thus low power (20-40W).

By increasing the SiH_4 flow rate, the number of Si-based radicals generated in the plasma increases and the deposited SiN_x layer be "Si-rich", and a composition closer to the substrate leads to less stress.The N_2 supplies the N atom for reaction. Decreasing the N_2 flow rate provides a "Si-rich" layer, and diminishes the residual stress as explained above. No significant influence of N_2 and SiH_4 flow rates on the deposition uniformity has been observed [19]. On the other hand, NH_3 has strong influence on the uniformity, perhaps because it provides the surface more hydrogen. Increase in the $NH_3\backslash SiH_4$ ratio creates tensile stress on the deposited film.

Typical pressure values are between 700 mTorr to 1100 mTorr. Decrease of the pressure results in an increase in electron energy which leads to an increase of the N/Si ratio and to compressive stress. On the opposite side, high tensile stress comes of the high pressures and given the fact that pressure influences the plasma stabilization [33], it has been concluded that a pressure around 900 mTorr could be optimal for SiN_x deposition, where the lowest residual stress is generated as well.

Last but not least, the influence of substrate's temperature needs to be discussed, which provides the kinetic energy in the species to diffuse and react. Its is well known by Fourier transform infrared spectroscopy (FTIR) analysis that the hydrogen concentration in PECVD SiN_x films decreases with the increase of temperature, scaling up from 100 ^oC to 250 ^oC [22]. Fur-

thermore X-ray photoelectron spectroscopy (XPS) has revealed that higher-temperature deposited films contain fewer defects, such as dangling bonds [22].

Many processes have been developed until now, aiming to achieve a low stress smooth SiN_x layer. Tarraf *et al.* [38] and Ven *et al.* reported on low and high RF frequency mix, showing that this alteration compensates the tensile stress, created by HF mode, with compressive stress, due to LF mode. Their results show low stress SiN_x. Loboda and Seifferly [26] introduced argon (Ar) into the process as a diluting gas. They found out that when Ar was added, the hydrogen incorporation was reduced and they could control the film stress. Finally, Mackenzie et *al.* [21] introduced helium (He) as an additional gas mixture changing the tensile stress to compressive. In the present work a comparison between HF and mixed-RF (HF-LF) modes has been made, for low plasma power (20 W), using 5% silane diluted in argon, NH_3 and N_2.

Chapter 6

Mask Patterning process

6.1 Electron Beam Lithography

The process of the mask transfer, including all steps and among of them them the EBL, is depicted in fig. 6.1. The steps could be summed up in three main phases: the material deposition, the electron beam lithography, and the selective etching.

Electron beam lithography is a fabrication technique that allow us to create patterns at nanoscale. The development of EBL tools started in the late 1960s by modifying the design of scanning electron microscopes. The working principle of EBL is very similar to photolithography. According to it, a focused beam of electrons scans across a substrate covered by electron-sensitive material (photo-resist). The pattern that we aim to transfer on the substrate is designed by a design software and indicates which areas will be illuminated, and which of them not. The electron beam changes the solubility properties only of the areas we wish to be removed/or remain (depending the tone of the photo-resist), according on the energy deposited by the electron beam.

A variety of different resists exists, with different properties that can be used as a resist for the lithography. One of the first materials developed for EBL was polymethyl methacrilate (PMMA) by M.Hatzakis in 1969 [16] and consists of the standard positive resists and one of the highest resolution resists available nowadays (fig. 6.2). Prior to EBL, the PMMA is spun on the substrate by a spincoater with a modulated thickness, which has been tested and proved to be adequate to the EBL exposure parameters. Immediately after the spincoating, the covered sample is baked at around 180^oC for the enhancement of the PMMA. For the PMMA being a positive photo-resist, this means that electron beam exposure breaks the polymer (i.e. changes the

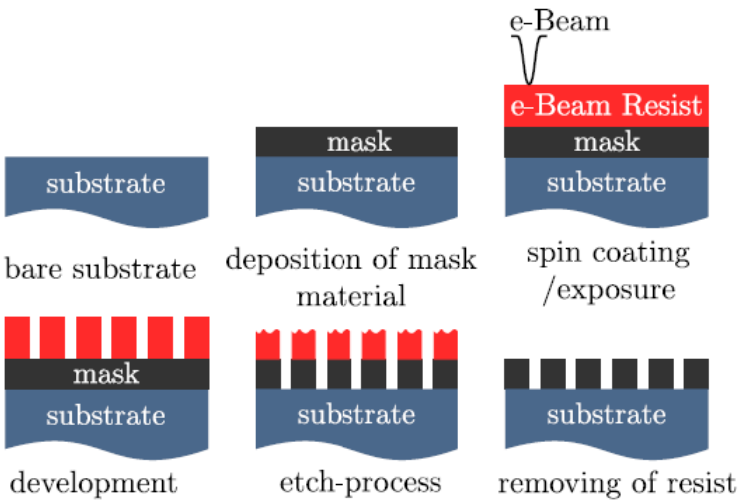

Figure 6.1: Procedure for the mask preparation by electron beam lithography

chemical structure) into fragments that can be dissolved in methyl-isobutyl-ketone (MIBK), the opposite holds for the negative photo-resist. While, both the exposed and unexposed PMMA can be dissolved in pirolide or acetone. MIBK is a too strong developer that can removes some of the unexposed resist as well, and for this reason, a mixture of MIBK to 3 parts isopropanol is usually used.

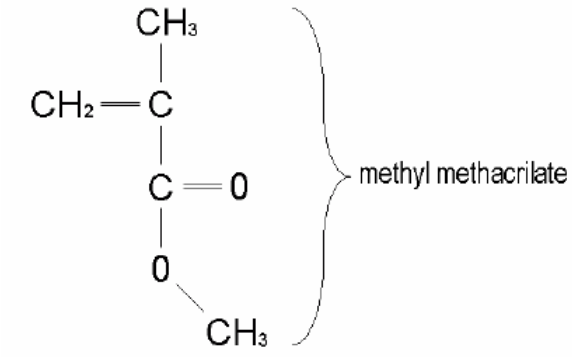

Figure 6.2: Chemical structure of methyl-acrilate (monomer of PMMA)

After the exposure, the exposed resist is washed away by the developer solution, leaving the patterned areas with the bare underlying mask material. After development, the Reactive ion etching is employed to etch down the exposed areas until the bare substrate is reached (in our case AlN). This is

the final step for the transfer of the patterned design onto the mask. During etching, PMMA protects the unexposed areas. The etching is dry and highly anisotropic, meaning that the etch is uni-directional. An anisotropic etch is critical for precise transfer of fine structures. For comparison, wet etching is isotropic a and causes undercutting of the mask layer by the same distance as the etch depth.

6.2 Reactive Ion Etching - RIE

In RIE, the substrate is placed inside a reactor where the etchant species are introduced. Using an RF power source, a plasma is generated in the gas mixture, breaking the gas molecules into ions. The ions are accelerated towards the surface and react with the substrate material, and the by-products desorb and are carried away of the system through a gas flow line. This is the chemical part of reactive ion etching. There is also a physical part which is similar in nature to the sputtering deposition process. If the ions have high enough energy, they can knock atoms out of the material to be etched without a chemical reaction. This physical process is responsible for the anisotropic etch, whereas isotropic etch is the result of the chemical processes. A schematic of a typical reactive ion etching system is shown in the figure below 6.3.

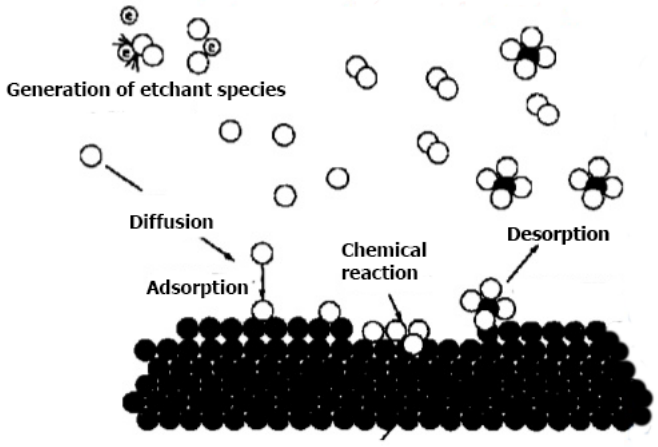

Figure 6.3: Schematic of the reactive ion etching process

CHF_3 is used to etch silicon nitride and the species produced in the plasma are CF_3 and CF_2 radicals. These radicals are poor etchants for other mater-

ials and this process is frequently choose to selectively etch silicon nitride on Si, GaAs, Al, W, Ti etch. CHF_3 alone has the tendency to form fluocarbon polymers [23], for this reason, a small amount of O_2 is added to suppress this. The addition of O_2 generates reactive species such as atomic O and atomic F. These species are good etchants for materials such as Si_3N_4, Si, and photoresist, and subsequently the selectivity of this process on this materials can be controlled by the addition of O_2. However, excessive O_2 oxidizes the SiN_x. An alternative solution could be CF_4/O_2 as used by Bertness et *al.*

Chapter 7

Gallium Nitride Nanocolumns

7.1 GaN properties

Gallium nitride is a III/V direct bandgap semiconductor with a wurtzite crystal structure. It has a direct band gap of 3.39 eV at room temperature (300^{o}C), which corresponds to the near ultraviolet, and lattice constants $a = 0.386$ nm, $c = 0.5186$ nm, as calculated at room temperature again. Moreover, it has a melting point of 2.500^{o}C. The wurtzite structure along with some primitive planes are depicted in Fig. 7.1

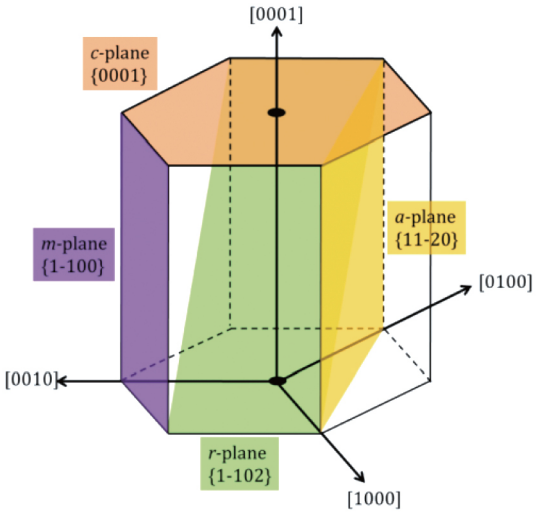

Figure 7.1: GaN unit cell and basic plaes c,a,m,r [25]

7.2 GaN nanocolumns

The term nanocolumns (NCs) and nanowire (NW) refer to the columnar growth of crystallites with height exceeding the diameter several times. For diameters below 100 nm the term nanowire is established, while for diameters above 100 nm and below 1 μm the term nanocolumn is used. The nanocostructures grown without a foreign catalyst are called self-induced and are the subject of this work.

Nanocolumns in general exhibit superior structural properties due to their large aspect ratio (surface to volume ratio). Unlike the epitaxial layer, the dislocations from the interface between the substrate and the nanocolumns, do not propagate, but they relax in the free side wall.

After the nucleation an the coalescence of the nanowires at the nucleation centres, the evolution of the WZ GaN nanoculmn starts by formating a- and m- planes, because their surface energy is lower than the other non polar crystal planes 11-13. A dodecagonal 6a/6m nanocrystal is thus promoted as seen in Fig. 7.2. The surface energy of the m-plane is somewhat lower than that of a-plane, driving the GaN nanocolumn to form the more thermodynamically stable hexagonal shape (6m facets). Once the hexagonal shape is reached, the GaN nanocrystal ends its morphological evolution [14]. Furthermore, if the tip of the nanocrystal is flat (c-plane surface) the nanocrystal is indentified to be N-polar. On the other hand, is it form a pyramidal tip, it is identifies as Ga-polar.

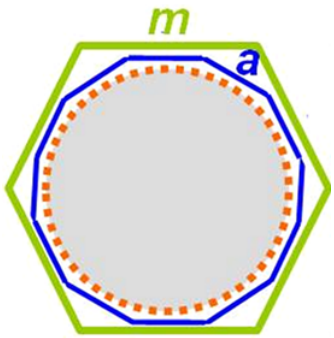

Figure 7.2: Evolution of the GaN nanocolumn from the circular nucleation centres to a- and m- crystal facets [14].

7.3 Growth mechanism

In order to investigate the growth mechanism of the nanocolumns, we need to consider the flux ratio of the reacting gases F_N/F_{Ga}, the growth time, the temperature of the substrate, the polarity, the substrate material as well as the masking material. The growth of self induced nanocolumns occurs under nitrogen-rich conditions at high temperatures (800^oC). .The mostly accepted and verified mechanism for GaN NW growth is based on total-energy density functional theory calculations, where it was estimated that at N-rich surface the Ga adatom migration barrier is four times higher than the Ga-rich condition and therefore is kinetically limited [35]. This induces the growth of three dimensional nuclei which eventually grow as NW at sufficiently high temperature. In the beginning, GaN nuclei accumulate and nucleate on the open areas. The nucleation may be delayed by and incubation time, which is the time needed for the growth of the critical nuclei. The incubation time, depends on the substrate's temperature and the Ga flux, and is in the ranges of tens of minutes and longer [39]. The size of the nuclei must exceed the critical value r_c that the Gibbs free energy of the system requires in order to continue to the NW growth. This is known as the elongation period. Once the critical nuclei are formed, next Ga adatoms coming onto the surface, diffuse onto the top of the NW from the side wall to minimize the chemical potential [32]. The kinetic energy needed to the Ga adatoms to diffuse, is provided by the substrate temperature. A shape transition from spherical cap-shaped to the hexagonal with m-plane sidewalls takes place during the elongation. The driving force for the shape transition is anisotropy of the surface energy among the polar, non polar and semipolar GaN surfaces [8]. The above description leads to the conclusion that nucleation stage is governed by thermodynamics, rather than kinetics. The elongation phase is governed by Ga diffusion toward the NW tip. In this kinetic description, in the axial growth contribute the directly impinging Ga and N adatoms, the diffusion on the substrate and the Ga diffusion on the sidewalls, all of them towards the tip. These conclusions came out of experiments. It is evidenced that the substrate temperature plays an important role in transforming the two dimensional compact layer into one nanowires growth with the same III-V ratio. GaN nanowires grow along the polar [0001] direction(c plane) exhibiting six fold surface symmetry. This is in agreement with the fact that the stable phase of GaN possesses hexagonal symmetry.

The dominant physical processes are Ga adatom surface diffusion from the surface towards the nanocoluns and/or Ga adatom desorption from the from the surface. The growth of self-induced and SAG GaN has been found to proceed under similar growth conditions as in the case of nanowires without

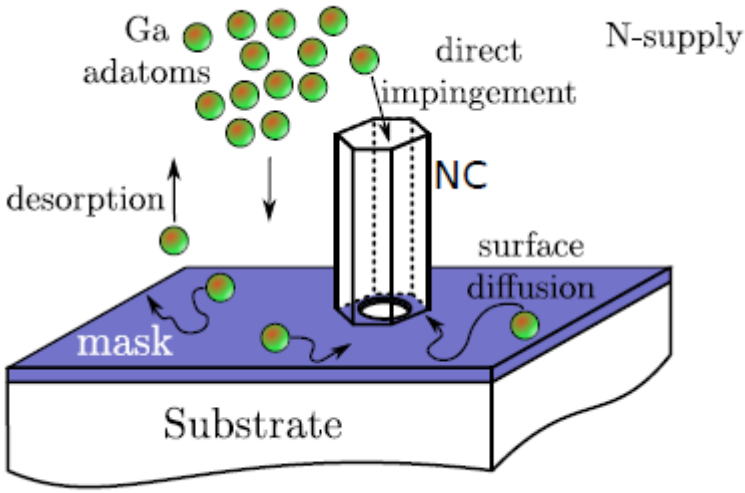

Figure 7.3: Scematic representation of the growth mechanisms in selective area growth NCs

the presence of a mask, and the sidewall morphology is comparable. This means that conceptual aspects that govern the self induced nanowires, should be taken into account also for the SAG nanocolumns: nucleation incubation times of GaN, Ga diffusion lengths, and changes of the magnitude of their contribution, due to the nanocolumn height [39]. The selective area growth epitaxy is the local growth of epitaxial layer or structure through a patterned dielectric or metal mask deposited on a substrate. The mask conditions are selected to ensure epitaxial growth on the exposed substrate, but not on the dielectric mask (fig. 7.3)

Part II

Results and growth optimisation

Chapter 8

Mask preparation

8.1 SiN_x thin film deposition

The PECVD reactor is a commercial PlasmaPro 100 PECVD System equipped with SiH_4 diluted in Ar in the percentage of 4%, N_2 and NH_3. The flow rare of the reactants is given in sccm, which denotes cubic centimeter per minute at STP. Both, mixed radio-frequencies mode and high frequency mode have been applied and a general investigation of the influence of the different parameters on the resulted surface has been made, concluding to optimization of the technique for the smooth thin films of silicone nitride. Two modes of deposition have been investigated, high frequency in the standard value of 13.56MHz, and mixed frequencies adding the low frequency of 380 kHz. The plasma power used is low (20 W) in order to achieve low deposition rates, which are needed for thin films. After deposition, every sample was scanned by atomic force microscopy (AFM) which gives an evaluation of the topography of the surface and an estimation of the overall surface roughness in root mean square (R_rms). R_rms is the root mean square average of the profile height deviations from the mean line, recorded within the evaluation length. The fields scanned are in size 4x4 μm. The pressure varied from 850 mTorr to 1000 mTorr and the temperature from 300^{o}C to 340^{o}C.

The process after placing the substrate into the load-lock chamber of the PECVD, includes an 1 min. pumpdown step, to restore chamber vacuum to base pressure. Follows a purge/pre-heat of the substrate lasting 5 min., to flush away any residual gases and ensure the wafer temperature has stabilised. Additionally, a plasma pre-clean step is added to clean the wafer surface and finally the PECVD process starts. The pre-clean plasma is important to avoid delamination of the films in cases that the film undergoes thermal or mechanical stress at a later stage in the process. The choice of plasma pre-

clean chemistry depends on the type of residue that needs to be removed from the wafer surface. Organic residues benefit from an N_2O pre-clean, whereas inorganic residues benefit from an NH_3/N_2 pre-clean. If a less chemical attack of the surface is required, then an N2 pre-clean can be used.

Representative surface morphologies are shown in Figs. 8.1, 8.3, 8.2, 8.4 for the samples indicated in table 8.1. An outlook of the results achieved in terms of roughness, indicates that PECVD technique provides quality thin films. No significant deference was observed between the two modes as seen from the AFM images and by the roughness obtained. This suggests that both techniques are more or less equal in the regime of low power investigated. In the case of low power, we expect that the N_2 is not evolved in a great percentage in the reactions, as it is more difficult to be activated. Therefore, we should expect SiH_n to react with itself and generate Si_2H_n by-products, that would supply the film with hydrogen leading to passivated bond and uniformity. If the supply of NH_3 is decreased as well, the reaction between the SiH_4 and NH_3 is further damped, enhancing the hypothesis that at the end, more hydrogen is accumulated on the surface. The above hypothesis is also supported by the deterioration of the surface morphology when decreasing the NH_3 flow rate from sample CR001 to sample CR003. However, when increasing the NH_3 flow rate, in the samples CR006-7, the surface deteriorates further. That can be attributed to radicals $Si(NH_2)_4$ and $Si(NH_2)_3$ that did not find a way to react and form Si_3N_4 due to low temperature. In the sample CR007, a trial to improve the surface morphology is succeeded by increasing the temperature, and decreasing the plasma pressure and increasing the nitrogen content. A decrease in the pressure was aiming to supply the electrons evolved in the plasma with kinetic energy to dissociate the nitrogen molecules. The surface morphology resulted in CR007, confirms this expectation. However, not specific attribute can be given. The surface roughness got the best value until that time achieved at 0.410 nm. Finally, a high temperature deposition took place, at 340^oC, with the flow rates given in Table 8.1 for CR008-9. The temperature is showing to highly promote the reaction of the radicals on the surface. Moreover, lower pressure, enhances the plasma reactions, contributing to the better roughness obtaining at CR009 at 0.377 nm. No further specific study took place, as the main topic was to obtain a good film morphology after understanding the basic effect of the parameters involved, and not a study of the reactions. For a further study, one could increase more the substrate temperature under the hypothesis that led to the parameters of CR007 sample. The surface obtained from the sample CR009, was satisfying and sufficient for a first test-mask for the growth of GaN NCs.

Taking the best deposition obtained (CR009), the deposition rate was estimated to be $\backsim$3.35 nm/min (Fig. 8.6). For the selective area growth,

	5% SiH_4 (sccm)	NH_3 (sccm)	N_2 (sccm)	Power (W)	P (mT-orr)	T(^{o}C)	dep. (mins)	rms (nm)
CR001	400	30	380	20-MRF	1000	300	5	0.735
CR002	400	30	380	20-HF	1000	300	5	0.643
CR005	400	30	380	20-MRF	900	300	10	1.296
CR006	400	30	380	20-HF	900	300	10	1.115
CR003	400	25	400	20-MRF	900	300	20	0.891
CR004	400	25	400	20-HF	900	300	10	1.2
CR007	400	20	600	20-MRF	850	320	5	0.410
CR008	400	30	380	20-MRF	1000	340	10	0.386
CR009	400	30	380	20-MRF	900	340	10	0.377

Table 8.1: Table with stuff

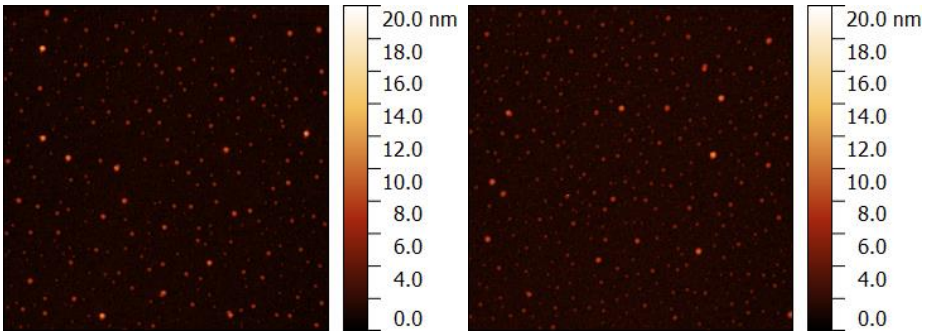

Figure 8.1: AFM topography for 5% $SiH_4/NH_3NH_3/N_2$ 400/30/380 respectively, 900mTorr, at 300^{o}C, MRF on the left - CR003, HF on the right - CR004

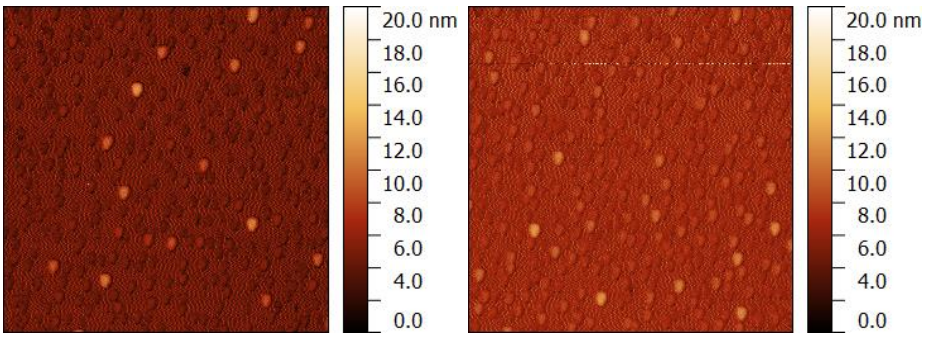

Figure 8.2: AFM topography for 5% $SiH_4/NH_3NH_3/N_2$ set to 400/30/380, 1000mTorr, at 300^{o}C, MRF on the left - CR005, HF on the right - CR006

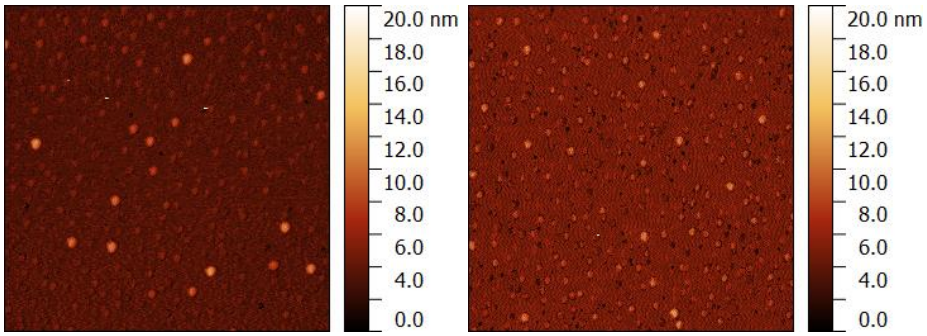

Figure 8.3: AFM topography for 5% $SiH_4/NH_3NH_3/N_2$ set to 400/25/400 respectively, 1000mTorr, at 300°C, MRF on the left - CR003, HF on the right - CR004

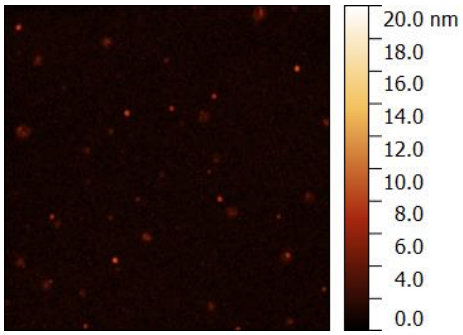

Figure 8.4: AFM topography for 5% $SiH_4/NH_3NH_3/N_2$ set to 400/20/600, 850mTorr, at 300°C, MRF - CR007

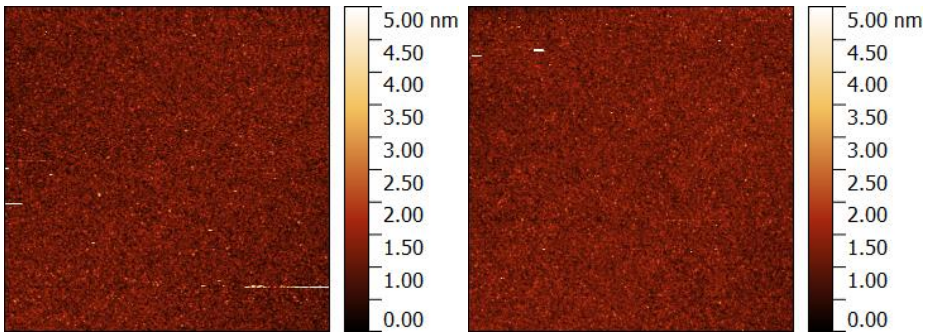

Figure 8.5: AFM topography for 5% $SiH_4/NH_3NH_3/N_2$ to 400/30/380, at 340°C, MRF mode, 1000mTorr on the left - CR008, 900mTorr on the right - CR009

the thickness of the mask can be as thin as possible and for this work it was chosen to be 10 nm. A thin mask has advantages over a thicker one, when it comes for the etching of the mask, at the step of the transfer of the mask pattern. A thicker mask needs more time to be etched on one

hand, and on the other, if the holes to be etched are small, the etchants will have a difficulty to reach down the substrate and probably a "bad quality", inhomogeneous pattern will be transferred at the end. Last but not least, in the case of a thick mask, the GaN nanocolumns will have to fill up the whole depth until they reach the surface, and then grow, which would be time-consuming, expensive, and it would serve no specific purpose. Therefore, 3 min. ($\backsim$10 nm) of SiN_x deposition was the standard process for the mask preparation.

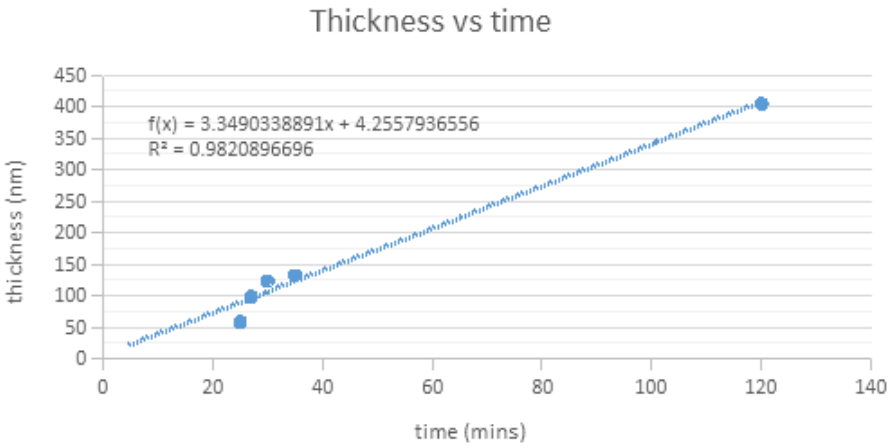

Figure 8.6: Thickness of SiN_x over time. Standard recipe:5% $SiH_4/NH_3NH_3/N_2$ to 400/30/380, at 340°C, MRF mode, 900mTorr.

The roughness of films deposited under the same conditions (as CR009 sample) but with varying deposition time was checked. As can be seen in Fig. 8.7, the surface deteriorates for longer times. However, until 25 min. deposition time, the surface roughness is in the range of 0.2-0.4 nm (R_rms), giving a reliability over the process and reproducible results.

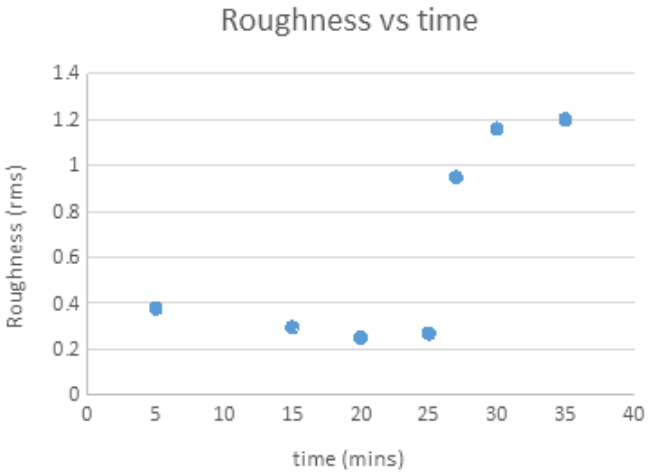

Figure 8.7: Roughness of SiN_x fims over time, for the standard recipe:5% $SiH_4/NH_3NH_3/N_2$ to 400/30/380, at 340°C, MRF mode, 900mTorr. The resulted surfaces are reproducible and the process is highly reliable.

8.2 SiN_x etching

For the etching of silicon nitride a standard recipe was used. At 55mTorr pressure, 50sccm CHF_3, 5sccm O_2, 150 W power, the average etching rate was found to be 104.68 nm/min (see diagram in Fig. 8.8). However, this etching rate does not concern the etching of patterned structures but the etching of free surface. Thus, longer etching time is expected to be needed.

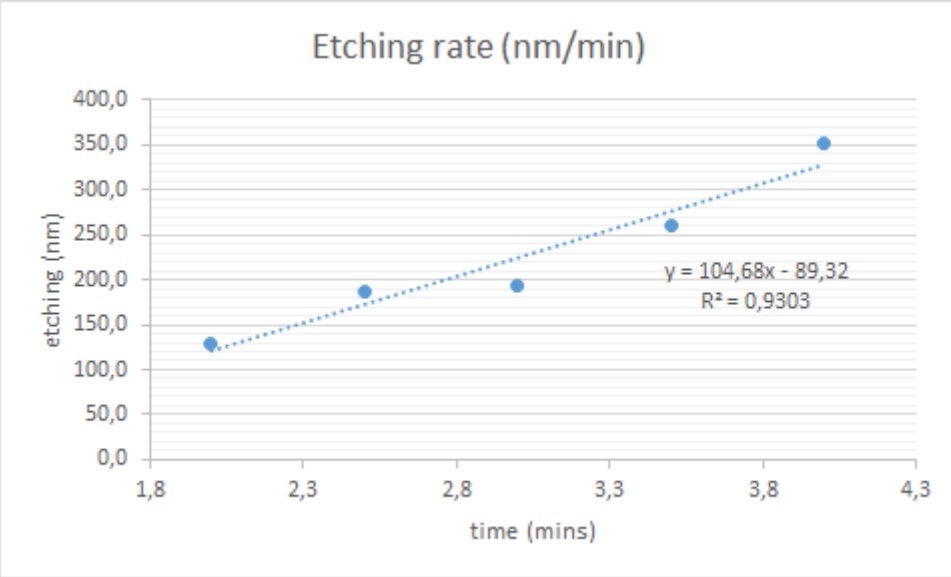

Figure 8.8: Etching of SiN_x over time. Standard recipe: 55 mTorr pressure, 50sccm CHF_3, 5sccm O_2, 150 W power.

Chapter 9

AlN buffer layer epitaxy

9.1 AlN buffer layer-Growth optimization of AlN bufer layers on Si(111)

1x1 cm. square wafers of Si(111) wafers were used as substrates for the AlN epitaxial growth. Prior the epitaxy, the wafers were solvent cleaned with aceton, methanol, and de-ionized water, for 2 min. each step, in ultrasonic bath, and then were blown dry with nitrogen to prevent stains from the drying solvents. The samples were then loaded into a molybdenun sample holder with molybdenum retaining clips and rings. The samples were outgased in the introduction chamber at 200 ^{o}C for 1h to outgas any remaining surface contaminants, such as moisture. The samples were then loaded into the buffer chamber where, again, they outgas at 600 ^{o}C, in lower pressure (10^{-9} mbar), for 3h and then they were loaded into the growth chamber of a Veeco Gen II MBE, equiped with a Veeco Unibulb rf plasma as a nitrogen source. This chosen times has been proved to be sufficient for a decrease of the backdround pressure while longer baking times result in carbon formation [5]. The plasma was operating at 1 sccm and 400W power. In the growth chamber, the samples underwent annealing until 1080^{o}C ($T_{thermocouple}$) to remove the thin surface oxide and then they were being cooled down slowly until the the 7x7 surface reconstruction takes place. The transition from 1x1 to 7x7 surface reconstruction appears at around 830^{o}C pyrometer temperature. Prior to epitaxy, a deposition of a few Al monolayers ($\backsim$5 sec.) was performed in all experiments. The growth temperature takes place at $\backsim$850^{o}C which has been proven high enough to supply the adatoms with kinetic energy to diffuse and give a better surface morphology. The sample holder was set to rotation mode at 5rpm during growth to provide homogeneous growth.

9.2 Nitorgen-rich conditions

To start with, a trial to delimit the two regimes, N-rich and Al-rich, in terms of aluminium flux, took place. For 3 samples grown at 1120, 1125, 1130, 1138^{o}C which correspond to $2.271 \cdot 10^{-7}, 2.481 \cdot 10^{-7}, 2.71 \cdot 10^{-7}, 3.06 \cdot 10^{-7}$ mbar beam equivalent pressure (BEP) the samples ended up with a rough surface and in columnar growth. This is an expected result, because as we go towards N-rich is the surface that the nanocolumns are The AFM topographies are shown in Fig. 9.1.

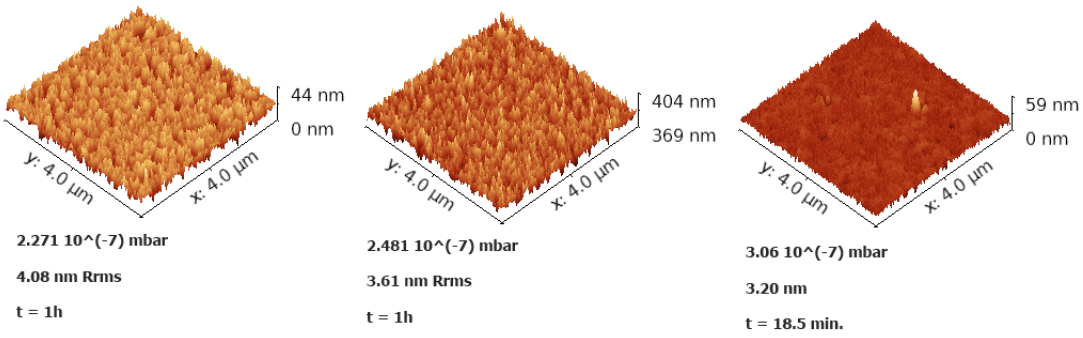

Figure 9.1: AFM topographies of samples grown at the nitrogen-rich regime

Going towards stoichiometry as can be seen, the growth of columnar structures is eliminated. A difference in the growth conditions should be mentioned in the samples shown in the Fig. 9.1. The right sample was grown on a Si(111)7x7 reconstruction surface, while the other two on Si(111)1x1. For the right one, it is remarkable how smooth is the surface in respect to the growth time which is only 18 min. comparing to the other two, that were grown for one hour.

9.3 Al-rich, on Si(111)1x1 surface, without Al consumption

In this set of samples prior to epitaxy, 5" of Al deposition took place at 990^{o}C. Right after, the temperature was increased to the growth temperature (850^{o}C) and the growth lasted about one hour. The result was a surface covered with metal droplets of 750 nm in diameter and larger, exceeding one micron. The surface roughness was 61 nm for sample (a) and 48 nm for sample (b) The surface that is covered by the droplets is smooth and exhibits around 1.7-2 nm R_{rms}. A method to get rid of the aluminium droplets is to

nitridate with plasma nitrogen the surface. However, in the case of large droplets, it is more difficult to ensure the consumption. For this reason, a combination of lower Al-fluxes with Al consumption is tried in the next samples prepared.

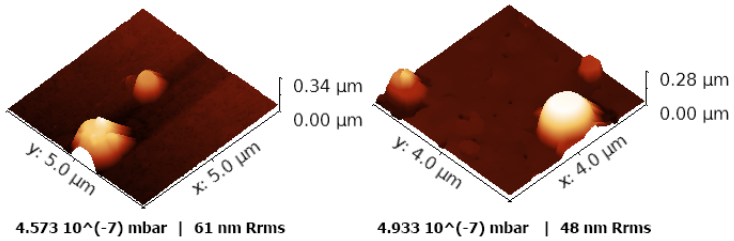

Figure 9.2: AFM topographies of samples grown on the Al rich regime, without other treatment at the end of the growth. The result is accumulation of droplets on the surface. Samples were grown for one hour and the fluxes tested are 4.573$\cdot 10^{-7}$ mbar BEP, and 4.933$\cdot 10^{-7}$ mbar

9.4 Al-rich, on Si(111)1x1 surface, with Al consumption

In the following three samples, the aluminium flux was kept constant at 3.77 $\cdot 10^{-7}$ mbar, and the growth time was one hour for a each sample. 5" of Al deposition was performed at 800^{o}C and then the growth started at the growth temperature of 850^{o}C. At the end of the growth, any metal on the surface got consumed by letting only plasma nitrogen impinge on the surface for approximately 10 min. during cooling down. The topographies are given in Fig. 9.3. The surface roughness is in the range of about 1.73-3.88 nm without any droplet accumulation - which is proved by the optical microscope check. However, the surface morphology is a subject of discussion. AFM images reveal surface full of corrugations or irregular sites that could possibly be the cause of additional dislocations and defects that would propagate and deteriorate the quality of the nanostructures.

9.5 Al-rich, on Al layer, without Al consumption

A really interesting come out was revealed when the next two samples were prepared. In this set, a few more monolayers of aluminium layers were de-

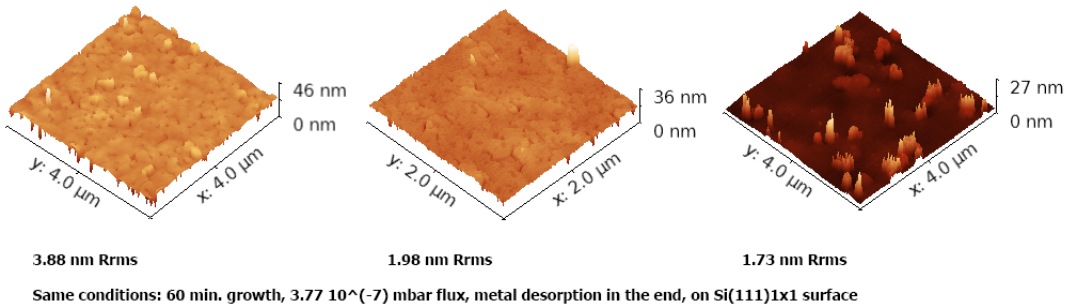

Figure 9.3: AFM topographies of samples grown slightly above stoichiometric point, at 3.175· 10^{-7} mbar BEP, for 12, 18, 20, 20 min.

posited at growth temperature (the depositing time was 50" and 37"). Then the growth took place in Al-rich conditions and lasted approximately one hour each. No nitridation was performed at the end of the experiment. The results were surprisingly good in the case of sample (a). The AFM revealed 3.7 nm R_rms for this sample and the optical microscope showed absence of metal droplets. The surface consists of a small number of threading dislocations and a few defects. Fig. 9.5 depicts the optical microscope image taken in the centre of the wafer in x100 magnification. In the case of the sample (b), the conditions were more Al-rich and the depositions the deposition of Al lasted 37". The optical microscope outcome was a surface with droplets, but not so big in size as in the case of less Al-deposition (compare to section 9.3). This gives a hint on the effect that the Si(111)1x1 is having on the epitaxy. It might be that the Si(111)1x1 surface reconstructs under the Al layer, however to support this, one should perform further diffraction studies.

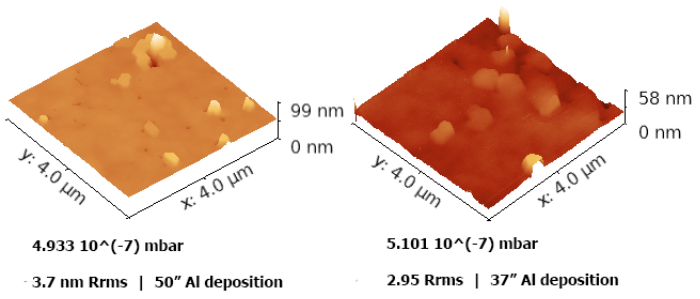

Figure 9.4: AFM topographies of samples grown in the Al-rich regime, above of a few Al layers, 4.933· 10^{-7} mbar (a) and 5.101· 10^{-7} mbar (5).

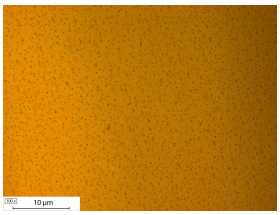

Figure 9.5: AFM topographies of samples grown slightly above stoichiometric point, at 3.175· 10^{-}7 mbar BEP, for 12, 18, 20, 20 min.

9.6 Near stoichiometric point, on Si(111)7x7 surface, with Al consumption

The samples that follow, were grown near stoichiometric point at fluxes of 3.175· 10^{-7} mbar BEP and 3.199· 10^{-7} mbar BEP -(a) and (b) respectively. Note that 3.06· 10^{-7} mbar BEP, is already in the N-rich regime, as tested in section 9.2. The sequence from top left to top right gives the evolution of the surface from the early stage of 12 min. to 20 min. Prior to epitaxy, a deposition of a few Al monolayers ($\backsim$5 sec.) was performed at around 790^{o}C pyrometer temperature. After that step, AlN starts at the same temperature as the Al deposition took place, gradually increasing the substrate temperature to the final one. This procedure was important so that the nucleation would start on the 7x7 reconstructed surface. The final growth temperature was at 850 ^{o}C pyrometer temperature. After the growth, post growth nitridation was performed. The samples grown are shown in Fig. 9.6. It can be seen that already in the early stage of 20 min., a smooth surface is achieved. The surface consists of threading dislocations, which in the image are identified by the small black "dots". The growth rate was calculated to be 351 nm/hour.

After investigating which conditions give good heteroepitaxial growth, we can conclude, based on observation, that growth on high temperatures, under slightly Al-rich conditions, and using the 7x7 surface as a starting point of the nucleation, give the smoother epitaxial growth.

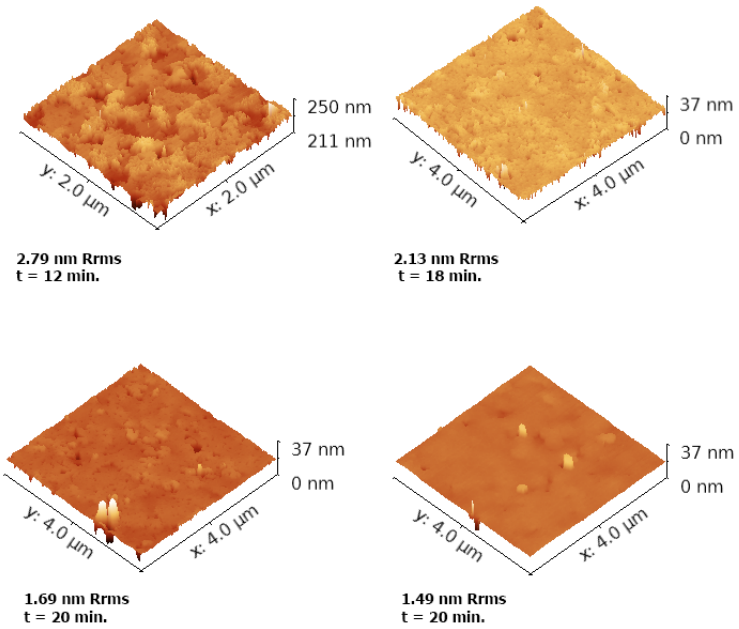

Figure 9.6: AFM topographies of samples grown slightly above stoichiometric point, at 3.175· 10⁻7 mbar BEP, for 12, 18, 20, 20 min.

Diameter variation, thermal stability al flux high, not zinc blend–¿ n-polar outgrowth. afm show diffusion.

Chapter 10

GaN nanowires

The mask was designed to have 10 fields of size 50x50 μm^2 each. The different sizes serve to give further information about the diffusion length of the adatoms on the mask. The pattern consists of circles of 500 nm (fields A-E) and 250 nm (fields F-J) in size, in array of a hexagonal structure. The distance between two consecutive circles from edge to edge is called pitch and has been selected to vary from 250 nm to 2μm as follows: 250, 500, 750, 1000, and 2000 nm.

The nucleation of the nanocolumns takes place under N-rich conditions. For N_2 plasma source at 1 sccm and 400 W power, the stoichiometric point was found to be at $5.64 \cdot 10^{-7}$ mbar BEP, for 800^{o}C substrate temperature. Due to lack of time no systematic observation of the nanocolumns took place and in the present section the achieves until now will be show. In the case of GaN NCs grown on GaN templates, the typical growth conditions, for plasma conditions of 1 sccm, 400 W, are III/V ration equal to 1/14 at 790^{o}C temperature. For a ration of III/V=1/14, 750^{o}C and growth of 3h, the nanowires reached only the starting point of coalescence (Fig. 10.1). This suggests that the Ga flux supplied for nucleation is low for these conditions. There is no nucleation in the area of the mask, and the structures dispose homogeneity. The nucleation of self-organised nanowires on the outer region of the mask, suggests that the desorption rate of the Ga from the mask is not high to prevent from nucleation on the mask.

At the next sample prepared, the Ga-flux was increased to 1/10, and 780^{o}C again for three hours. These conditions resulted in more closed structures and good selectivity. Up to 1 μm pitch (see D field, Fig. 10.2) the mask is almost free of parasitic nucleation. However the quality of NCs is not good, as the lateral growth deviates - the base of the nanocolumns have not uniform hexagonal shape. The growth in the different fields, with only variable being the pitch, can be seen in Fig. 10.3. The structures are more or

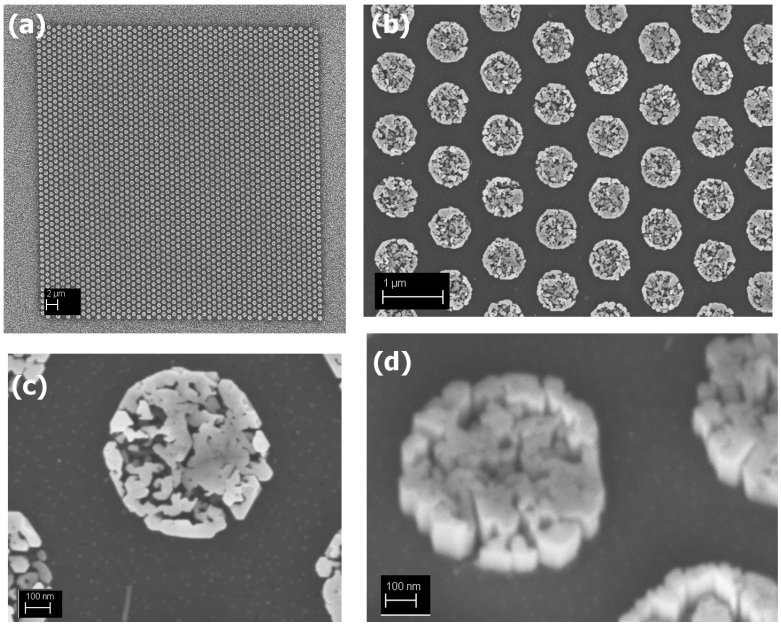

Figure 10.1: Scanning electron microscopy (SEM) of GaN NCs grown at III/V=1/14, T=750^{o}C.

less similar and uniform, however they appear to have a porous morphology with unfilled regions inside. This is a sign of not enough Ga supply again.

Going to 1/4 ratio and 804^{o}C the mask does not show any parasitic nucleation except from defects on the mask that served as nucleation centres. Regarding the nanocolumns, they are not closed yet and they appear to have larger voids in the middle. This is reasonable, because the higher substrate temperatures decrease even more the time that the Ga adatoms spend on the surface and the probability to diffuse and incorporate on the nanocolumns (Fig. 10.4).

The ratio of 1/2.5 and slightly higher temperature (810^o) and 6h growth showed parasitic nucleation even for the small pitches. Still, the nanocolumns of 500nm nominal diameter, appear to have incomplete haxagonal tips, which in this case it can be due to desorption or even decomposition. However, it is of great importance the fact that for the fields prepared with diameters of 250 nm, the tips appear to close. This observation leans to the suggestion that the voids appearing for larger diameters are indeed due to insufficient Ga effective flux, prevailing us from doing any hypothesis for defects. The effective Ga flux is the sum of all the components that contribute to incorporation and growth: direct supply of Ga adatoms and diffusion from the mask in this case. If we neglect the diffusion from the mask due to low contribution, flux

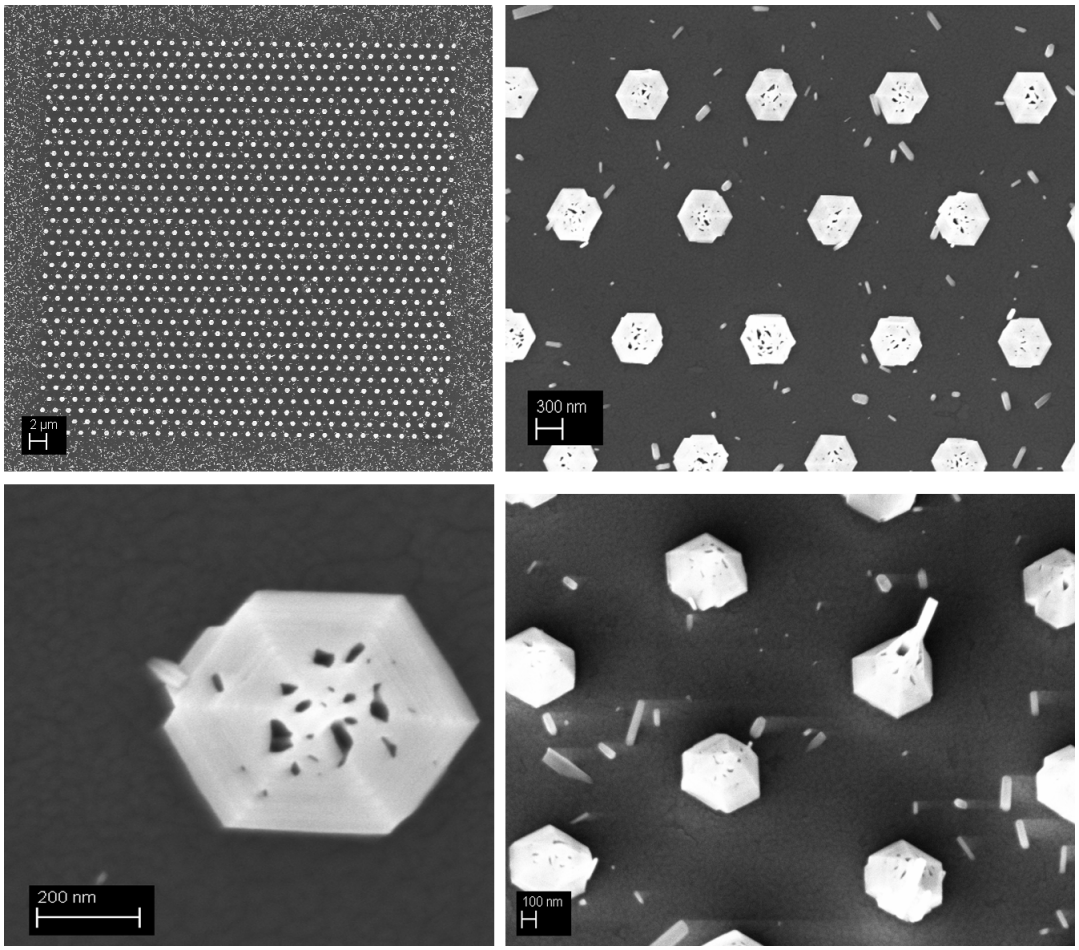

Figure 10.2: D field (d=500 nm, p=1 µm) of nanocolumns grown at 1/10 flux ration and 780º C.

F_N/F_{Ga}^{eff} shift to more nitrogen-rich conditions and thus to low growth rates. This is also consistent with the appearance of only pyramidal structures.

Finally, the stability of the mask was checked for 830ºC where it got decomposed (see Fig 10.5). This temperatures are in the region where GaN already decomposes, which ensures the thermal stability of the mask under GaN growth conditions.

A difference and that this work exhibits in comparison to GaN grown on GaN template with metal mask, is that the resulted fields have homogeneity from the centre towards the edges. This could be a result of different thermal conduction that SiN_x provides (Fig. 10.6, 10.7). Furthermore, it has been observed that Mo mask is not thermally stable in high temperatures, which temperatures, are useful to modulate the diffusion on the mask and as a

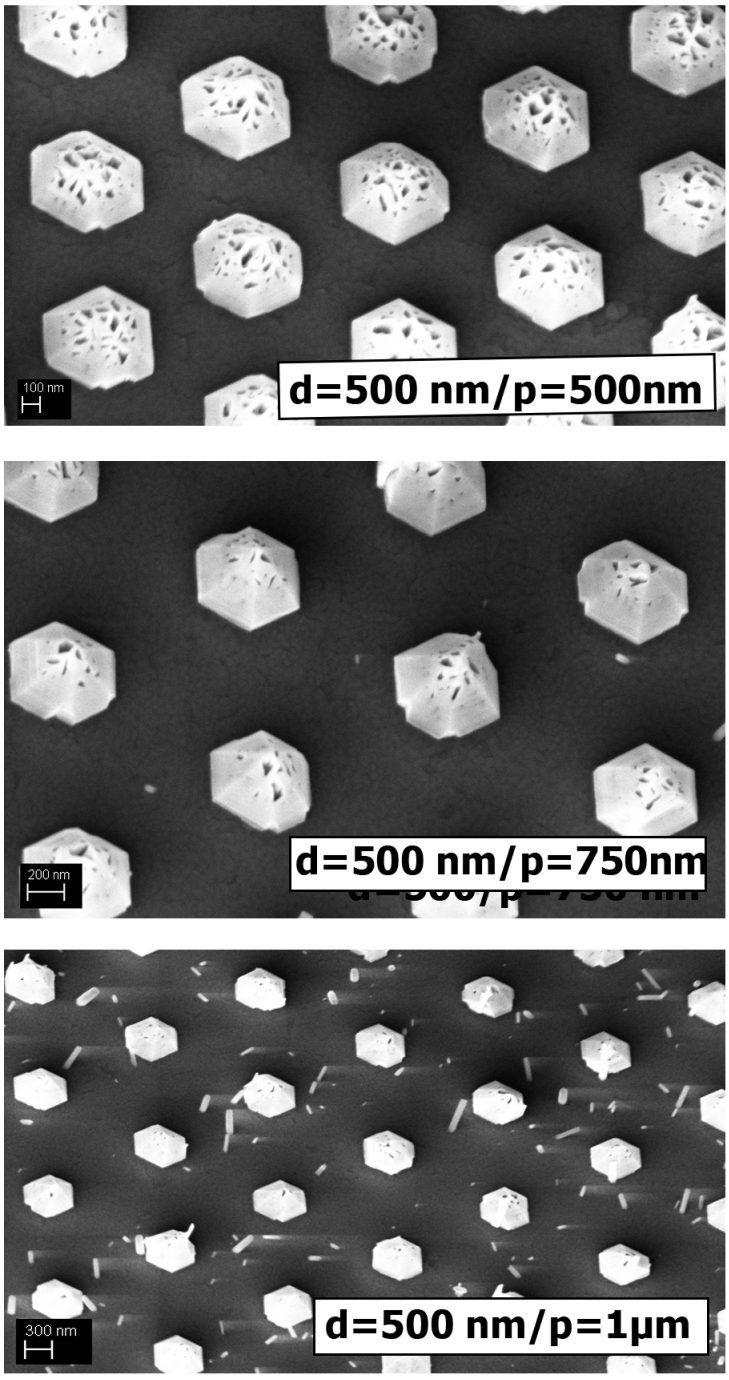

Figure 10.3: Tilted by 40º of the B, C and D fields of nanocolumns grown at 1/10 flux ration and 780º C.

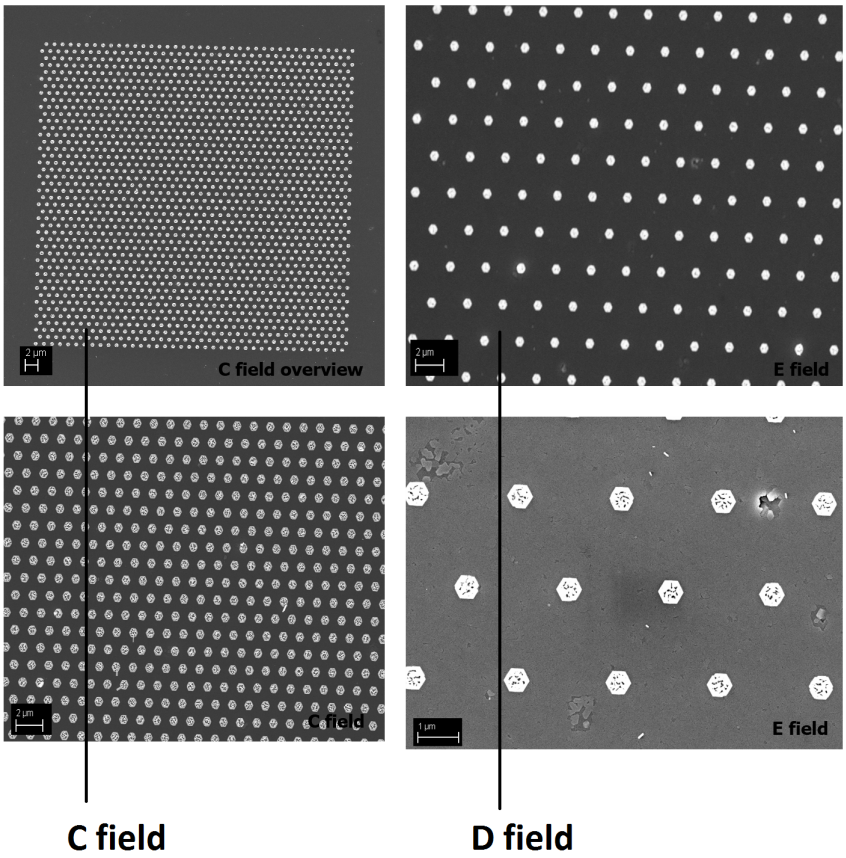

Figure 10.4: C and D fields of sample grown at 804°C and at ratio 1/4. The growth is homogeneous and the mask shows no parasitic nucleation.

consequence the parasitic nucleation.

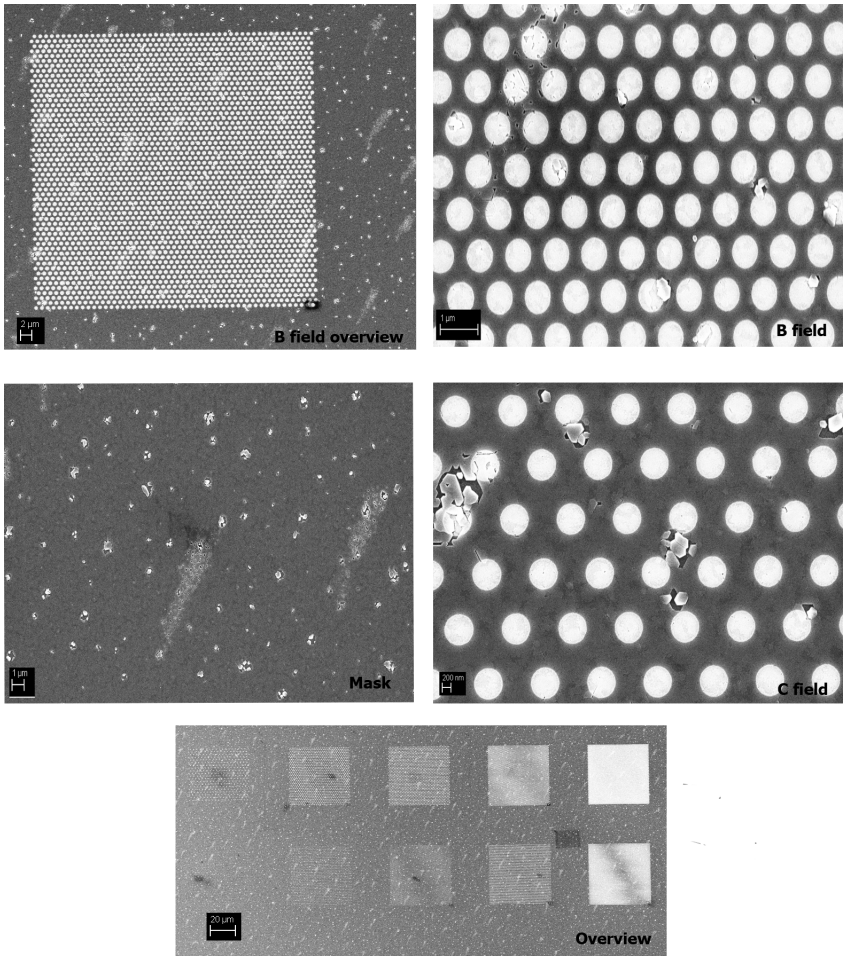

Figure 10.5: The mask decomposes at 830°C which is excessively high for GaN nanocolumn growth.

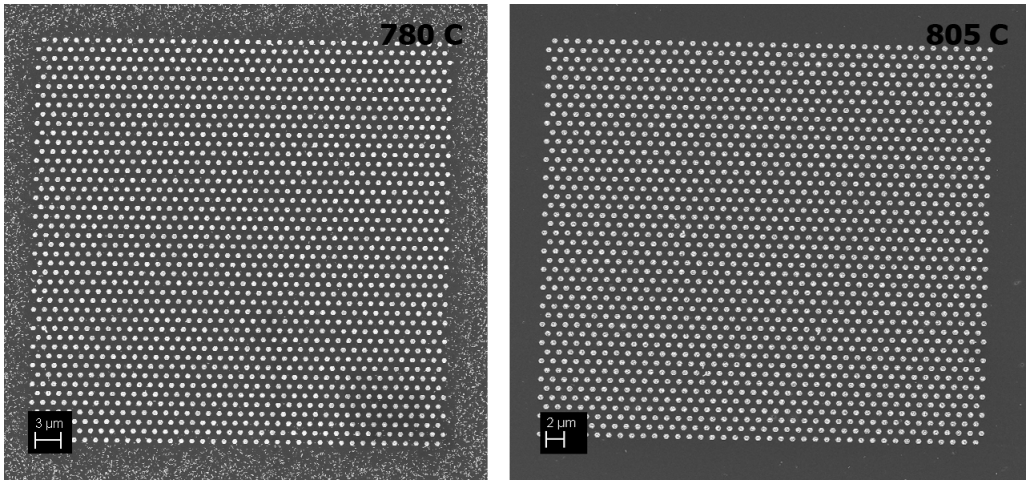

Figure 10.6: C fields for temperatures of 780º C and 805º C. The fields show absolute homogeneity.

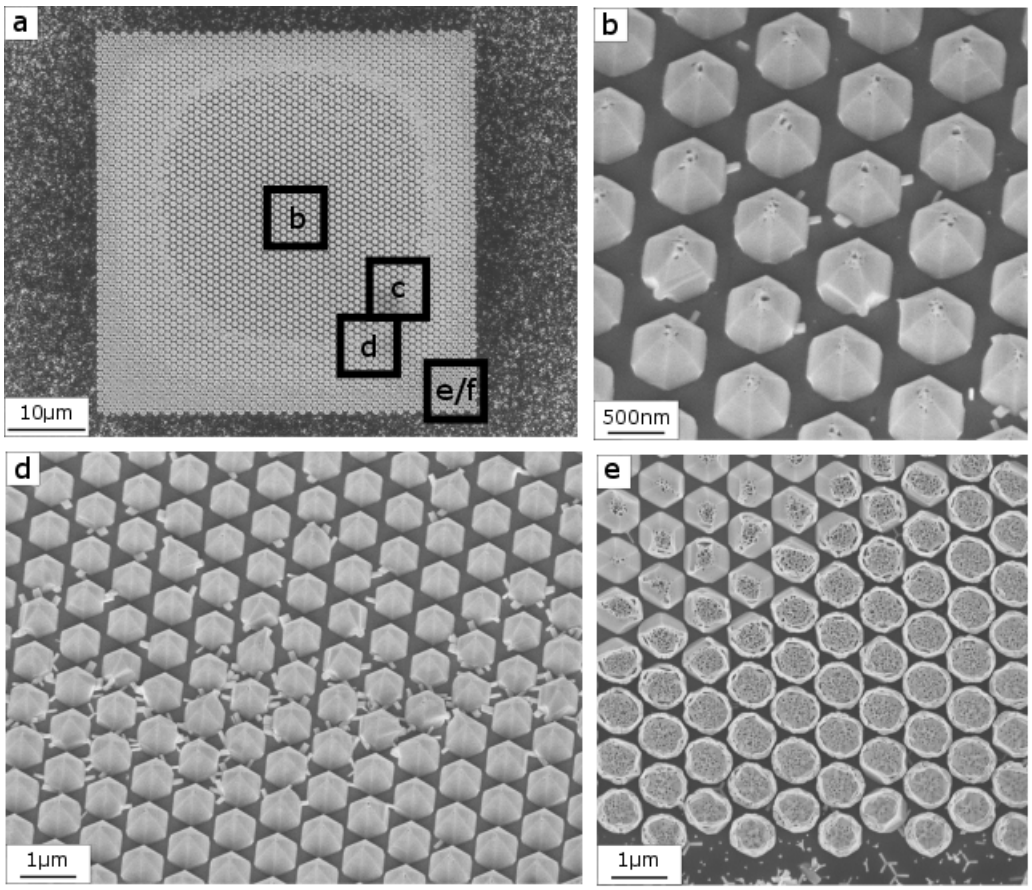

Figure 10.7: Results of EBL mask in size 50x50 µm, for GaN grown on GaN with metal masks. This set depicts the inhomogeneities that this growth exhibits. The results are taken by the master thesis of Henning [17].

Chapter 11

Outlook

In this thesis a brief introduction in the theory of epitaxial growth, along with the experimental growth of layers and nanocolumns is taking place. Growth conditions in MBE for III-nitrides are driven by the substrate temperature, the nitrogen flux and the metal flux. A smooth epitaxial layer of AlN is achieved observing the RHEED pattern to monitor the growth conditions. Based on observation, slightly above stoichiometry conditions (Al-rich) produce the best results in terms of crystal quality and surface morphology. A dependence of the AlN surface morphology to the appearance of the Si(111)7x7 surface reconstruction is observed. Layers grown on Si(111)7x7 result in a smooth surface with a few threading dislocations, whereas, layers grown on Si(111)1x1, result again in roughness but the morphology of the surface consists of corrugations or irregular sites.

Meanwhile, the chemical deposition under plasma conditions for thin films is studied. The reactions that occur during PECVD are complex, however, a study on the effect that they have on the strain of the wafer and on the uniformity, have been investigated by research groups previously [19]. In this this work, the process of thin film deposition of SiN_x is established. The process has high reproducibility and produces thin films with R_{rms} between 0.3-0.4 nm. No significant change has been observed between high frequency mode and mixed-mode (high and low frequency), which can be attributed to the low power used, which generates low energy electrons in the plasma an thus, NH_3 dissociation is not promoted, which would lead in unsaturated hydrogen bonds on the surface in the case of high power.

Finally, the GaN NCs growth has been observed with the SiN_x mask. SiN_x is proved thermally stable under GaN NCs growth conditions. The morphology of the structures grown is pyramidal and exhibits voids in the middle. In the growth temperatures studied, the contribution of diffusion from the surface is small, almost negligible, because the diffusion is limited

by evaporation. The directly impinging Ga adatoms nucleate on the holes and build they seem to prefer the incorporation at the outer regions first, leaving voids on the centre of the structure. Pyramidal structures with no axial growth exists in the regime of the excessive nitrogen-rich conditions (ratio 1/14), but this ratio takes into account also diffusion from the mask. If we neglect this component then the ratio shifts to even more nitrogen-rich conditions, explaining the unclosed tips. This is confirmed by the existence of closed tips in the case of 1/2.5 ratio and diameters of 250 nm (sample G1915).

Comparing the SiN_x mask with previously studies Ti, or Mo masks [17], the mask seems to provide better homogeneity on the growth, as the conditions in the fields does not change from the outer regions to the centre. For the set of experiments performed, no irregular shapes have been observed, except from same random nuclei grown perpendicular inside the body of the structures. Further experimental series, are needed to optimise these new growth conditions. However, so far, they seem promiscuous, because if the system is, in the end, only affected by the direct imping of adatoms, this would make the growth much more manipulative and not complex. Finally, the Si substrate is advantageous over GaN templates because it is not transparent and therefore, controlling the temperature of the substrate by a pyrometer becomes easier.

For further studies, a try to modulate the impinging flux is necessary, in order to obtain closed tips. Photoluminescence experiments will show further if the nanocolumns are of high quality or not, and a mask design with different diameters of holes, would be ideal to show the growth evolution of the nanostructures.

Appendix

Details regarding electron beam lithography

After growing an AlN buffer layer on silicon wafers, a 10nm thin film of SiN_x is deposited as the mask material and the samples proceed to electron beam lithography.

Before performing electron beam lithography, the samples are spincoated with the resist. First they are cleaned with aceton and isopropanol in ultrasonic bath and they are blown dry with N_2. Then the samples are loaded into the spincoater with the photoresist. The resist used is the AR-P679.04 and the spincoating process was operating at 7000 rpm, 800 ramp, for 60 sec. Immediately after spincoating, the samples were baked at 180^oC for 5mim., for the resist to dry. This recipe works to give approximately a 260 nm thick of the above resist on a SiN_x surface. This thickness has been chosen in agreement with the parameters of the EBL. The samples then are loaded to EBL which illuminates the circles in hexagonal array previously designed. EBL operates at 20 kV voltage, 20 μm aperture, 350 $\mu As/cm^2$ area dose. After EBL the samples are developed in MIBK/IPA 1:3 for 30 sec. and they are dissolved in isopropanol for 30 more sec. The developer, as discussed, removes the illuminated parts and the SiNx is revealed at the bottom. The samples are then etched down at RIE, and afterwards, they are being dissolved in NEP for 30 min., to remove the resist that was not illuminated. Regular cleaning if following the NEP with aceton, methanol and water in ultrasonic bath, and the samples are ready to grow.

Acknowledgements

I would like to express my deep gratitude to Professor Angela Rizzi and Joerg Malindretos, for their patient guidance, enthusiastic encouragement and useful critiques of this research work. I would also like to thank Prof. George Papaioannou my supervisor and Spiros Gardelis, for their advice and assistance in keeping my progress on schedule, as well as, for being members of the three-member committee.

I would also like to extend my thanks to the technician of the laboratory Thomas Leeman, for his help in offering me the resources in running my experiments.

I would like to express my very great appreciation to my colleagues, Christian Diestel, Philipp Henning, Stephan Behrenz, Marcel Kroener, Klaas Strempel for their valuable and constructive suggestions, during the planning and development of this research work.

Finally, I wish to thank my parents for their support and encouragement throughout my study, and my beloved George.

Bibliography

[1] T Babinec. A diamond nanowire single-photon source Thomas. *nature nanotechnology*, 5:195–199, 2010.

[2] L. Bdoš, J. Musil, and M. Lubański. Chemiluminescence of the silane - Active nitrogen reactions during PECVD of the silicon nitride films. *Czechoslovak Journal of Physics*, 1984.

[3] A Bourret. Growth of aluminum nitride on (111) silicon: Microstructure and interface structure. 83(4):2003–2009, 1998.

[4] A. Bourret, A. Barski, J. L. Rouviere, G. Renaud, and A. Barbier. Growth of aluminum nitride on (111) silicon: Microstructure and interface structure. *Journal of Applied Physics*, 83(4):2003, 1998.

[5] Daniel Broxtermann. *Towards high electron mobility in GaN (0001) based InGaN and AlGaN heterostructures*. PhD thesis, 2011.

[6] Shawn D Burnham, Gon Namkoong, Kyoung-Keun Lee, and W Alan Doolittle. Reproducible reflection high energy electron diffraction signatures for improvement of AlN using in situ growth regime characterization. *Journal of Vacuum Science & Technology B J. Appl. Phys*, 25(93), 2007.

[7] Julien Claudon. A highly efficient single-photon source based on a quantum dot in a photonic nanowire. *nature photonics*, 4:174–177, 2010.

[8] V. Consonni, M. Knelangen, L. Geelhaar, A. Trampert, and H. Riechert. Nucleation mechanisms of epitaxial GaN nanowires: Origin of their self-induced formation and initial radius. *Physical Review B - Condensed Matter and Materials Physics*, 2010.

[9] Dan Dalacu, Khaled Mnaymneh, Vera Sazonova, Philip J. Poole, Geof C. Aers, Jean Lapointe, Ross Cheriton, Anthony J. Springthorpe, and

Robin Williams. Deterministic emitter-cavity coupling using a single-site controlled quantum dot. *Physical Review B - Condensed Matter and Materials Physics*, 2010.

[10] B Daudin and F Widmann. Layer-by-layer growth of AlN and GaN by molecular beam epitaxy. *ELSEVIER Journal of Crystal Growth*, 182:1–5, 1997.

[11] Parijat Deb, Hogyoung Kim, Vijay Rawat, Mark Oliver, Sangho Kim, Mike Marshall, Eric Stach, and Timothy Sands. Faceted and vertically aligned GaN nanorod arrays fabricated without catalysts or lithography. *Nano Letters*, 2005.

[12] Ch. Gerber G. Binnig, H. Rohrer and E. Weibel. title.

[13] L. Geelhaar H. Riechert W. Hsler G. Koblmueller, R. Averbeck and P. Pongratz. Growth diagram and morphologies of aln thin films grown by molecular beam epitaxy.

[14] Z Gacevic. Formation mechanisms of gan nanowires grown by selective area growth homoepitaxy. *Nano Letters*, 15(2):1117–1121, 2015.

[15] Matthew T. Hardy, Daniel F. Feezell, Steven P. Denbaars, and Shuji Nakamura. Group III-nitride lasers: A materials perspective. *Materials Today*, 2011.

[16] M. Hatzakis. Electron Resists for Microcircuit and Mask Production. *J. Electrochem. Soc*, 116(7):1033–1037, 1969.

[17] P Henning. *Selektives Wachstum von Ga-polaren GaN-Nanosäulen Selective Area Growth of Ga-polar GaN Nanocolumns Philipp Henning*. PhD thesis, Go, 2016.

[18] Dennis Hess. Plasmaenhanced CVD: Oxides, nitrides, transition metals, and transition metal silicides. *Journal of Vacuum Science & Technology A*, 2:244–252, 1984.

[19] Ciprian Iliescu, Francis E H Tay, and Jiashen Wei. Low stress PECVDSiN x layers at high deposition rates using high power and high frequency for MEMS applications. *J. Micromech. Microeng*, 16:869–874, 2006.

[20] S Keller. Optical and structural properties of GaN nanopillar and nanostripe arrays with embedded InGaNGaN multi-quantum wells. *Journal of Applied Physics*, 100(054314), 2006.

[21] Mike DeVre Russ Westerman Ken Mackenzie, Brad Reelfs and Dr. Dave Johnson. Optimization of low stress pecvd silicon nitride for gaas manufacturing.

[22] Yue Kuo and Hyun Ho Lee. Plasma-enhanced chemical vapor deposition of silicon nitride below 2501C. *Vacuum*, 66:299–303, 2002.

[23] J. W. Lee, K. D. Mackenzie, D. Johnson, S. J. Pearton, F. Ren, and J. N. Sasserath. Development of Low Temperature Silicon Nitride and Silicon Dioxide Films by Inductively-Coupled Plasma Chemical Vapor Deposition. *MRS Proceedings*, 573:69, 2011.

[24] R Liu, F A Ponce, A Dadgar, and A Krost. Atomic arrangement at the AlN/Si (111) interface Interface properties of Al x Ga 1x N/AlN heterostructures from optical waveguiding information Atomic arrangement at the AlNÕSi " 111... interface. *Citation: Applied Physics Letters Appl. Phys. Lett. Appl. Phys. Lett. Phys. Lett. Appl. Phys. Lett. Phys. Lett*, 83(74):11910–251901, 2003.

[25] Zhang Jian-Li Liu Jun-Lin. Status of gan-based green light-emitting diodes.

[26] Mark J. Loboda. Chemical influence of inert gas on the thin film stress in plasma-enhanced chemical vapor deposited a-sin: H films.

[27] Helmut Sitter Marian A. Herman. *Molecular Beam Epitaxy: Fundamentals and Current Status*.

[28] Ivan V. Markov. *Crystal Growth for Beginners: Fundamentals of Nucleation, Crystal Growth, and Epitaxy.*

[29] Shuji Nakamura, Takashi Mukai, and Masayuki Senoh. Candela-class high-brightness InGaN/AlGaN double-heterostructure blue-light-emitting diodes. *Applied Physics Letters*, 64(13):1687–1689, 1994.

[30] Xin-Qiang Guang Chen Liu Shi-Tao Feng Li Fu-Jun Xu Tang Ning Shen Bo Pan, Jian-Hai Wang. Epitaxy of an al-droplet-free aln layer with step-flow features by molecular.

[31] M Pelton. Efficient Source of Single Photons: A Single Quantum Dot in a MicropostMicrocavity Matthew. *Physical Review Letters*, 89(23):2336021–2336024, 2002.

[32] T. Richter T. Stoica R. Calarco R. K. Debnath, R. Meijers and H. Luth.

[33] Donald Smith. Controlling the plasma chemistry of silicon nitride and oxide deposition from silane. *Journal of Vacuum Science & Technology A*, 11:1843–1849, 1993.

[34] G.-C. Wang T. Karabacak, Y.-P. Zhao and T.-M. Lu. Growth front roughening in silicon nitride films by plasma-enhanced chemical vapor deposition.

[35] J. Neugebauer T. Zywietz and M. Scheffler. Adatom diffusion at gan (0001) and (0001) surfaces.

[36] Kunio Takayanagi, Yasumasa Tanishiro, Shigeki Takahashi, and Masaetsu Takahashi. Structure analysis of Si(111)-7 7 reconstructed surface by transmission electron diffraction. *Surface Science*, 1985.

[37] Yoshitaka Taniyasu and Makoto Kasu. Improved emission efficiency of 210-nm deep-ultraviolet aluminum nitride light-emitting diode. *NTT Technical Review*, 2010.

[38] A Tarraf, J Daleiden, S Irmer, D Prasai, and H Hillmer. Stress investigation of PECVD dielectric layers for advanced optical MEMS. *J. Micromech. Microeng. J. Micromech. Microeng*, 14(14):317–323, 2004.

[39] Arne Urban. Position-controlled selective area growth of Ga-polar GaN nanocolumns by molecular beam epitaxy : A versatile approach towards semipolar GaN and the characterization of single nanocolumns Dissertation. 2013.

[40] Junqiao Wu. When group-III nitrides go infrared: New properties and perspectives. *Journal of Applied Physics*, 106(011101), 2009.